Site Specific Probabilistic Seismic Hazard Model for Isfahan, Iran: Estimates and Uncertainties

Mohsen Kohrangi (mohsen.kohrangi@gmail.com)
RED, Risk Engineering and Development https://orcid.org/0000-0001-9151-0361
Homayon Safaei
University of Isfahan
Laurentiu Danciu
University of Zurich: Universitat Zurich
Hossein Tajmir-Riahi
University of Isfahan
Rassoul Ajalloeian
University of Isfahan
Paolo Bazzurro
IUSS: Scuola Universitaria Superiore Pavia

Research Article

Keywords: Probabilistic Seismic, hazard spectra, Earthquake

Posted Date: November 17th, 2021

DOI: https://doi.org/10.21203/rs.3.rs-851455/v1

Version of Record: A version of this preprint was published at Bulletin of Earthquake Engineering on March 14th, 2022. See the published version at https://doi.org/10.1007/s10518-022-01373-4.

Abstract

We present a seismic source characterization model for the probabilistic seismic hazard assessment (PSHA) of the Isfahan urban area, Iran. We compiled the required datasets including the earthquake catalogue and the geological and seismotectonic structure and faults systems within the study region to delineate and characterize seismic source models. We identified seven relatively large zones that bound each region with similar seismotectonic characteristics and catalogue completeness periods. These regions were used for calculating the *b*-value of the Gutenberg-Richter magnitude recurrence relationship and for estimating the maximum magnitude value within each region. The recurrence parameters were then used to build a spatially varying *distributed seismic source model* using a smoothed kernel. Additionally, based on a fault database developed in this study and on a local expert's opinion about their slip velocity, *an active faults* based model is also created. We further performed sets of sensitivity analyses to find stable estimates of the ground motion intensity and to define alternative branches for both the seismogenic source and ground motion prediction models. Site amplification is considered based on a Vs_{30} map for Isfahan compiled within this study. The alternative source and ground motion prediction models considered in the logic tree of this study are then implemented in the software Open Quake to generate hazard maps and uniform hazard spectra for return periods of interest. Finally, we provide a detailed comparison of the PSHA outcomes of the current study both with those presented in the 2014 Earthquake Model of Middle East (EMME14) and with the national seismic design spectrum to further discuss the discrepancies between hazard estimates from site-specific and regional PSHA studies.

1. Introduction

Probabilistic seismic hazard analysis (PSHA) (Cornell 1968; McGuire 2004) is the standard procedure for estimating the ground shaking hazard at a site (McGuire 2004). The nature of the phenomenon dictates the application of probabilistic approaches to blend information about seismic sources, earthquake magnitudes, seismic wave traveling paths, the estimates of the ground motion intensity and site response with the information about the historical earthquakes and seismotectonic settings with the objective of estimating the likelihood of observing future ground motion intensities at a site. In other words, PSHA considers "all" earthquake scenarios that can affect a given site combined with the distribution of ground motion intensity (commonly defined through ground motion prediction equations, GMPEs) to be expected at the site for all such earthquake scenarios, to quantify the probability of exceeding different levels of ground motion intensity measures, such as peak ground acceleration (*PGA*) and spectral acceleration (*Sa*). Estimating seismic hazard analysis is essential for developing resilient cities in seismic prone areas because it provides the fundamental requisite for the design of new safe buildings and for the assessment of the existing ones.

Iran as one of the most seismically active regions in the Middle East, has a long history of hazard studies starting from early sixties. Since 1962 to date different versions of the seismic design guidelines and codes have been adopted country-wide. The latest version of the seismic design code (i.e., fourth edition of Standard 2800) indicates the level of seismicity for different regions of the country based on a seismic zonation map (ICSRDB 2014; Moinfar et al., 2012). Besides Standard 2800, two regional hazard studies of GSHAP (Giardini 1999) and EMME14 project (Şeşetyan et al. 2018; Danciu et al. 2016b) also include Iranian territory. Several studies conducted hazard studies specifically for Isfahan urban area including identification of active faults and performing hazard analysis (Beygi et al. 2016; Safaei et al. 2012; Tabaei et al. 2016; Tajmir Riahi et al. 2014).

In this paper, we describe a probabilistic seismic hazard model developed for Isfahan following the concepts and methodologies set by Field et al. (2003) implemented in the OpenQuake engine (Pagani et al. 2014). Our model is based on the latest information in openly accessible datasets and scientific literature and we supplemented it with local experts' judgement. The model consists of a combination of distributed seismicity areas and active faults within the region. The former is underpinned by the direct analysis of earthquake catalogues, while the latter is based on the spatial delineation and activity rates of faults derived by geological and geodetic observations. We intend to combine these two source models to address the limitations of each and to explicitly account for epistemic uncertainties of various modelling approaches to produce a robust estimate of the seismic hazard in the urban area of Isfahan. We also discuss our model development assumptions and the corresponding implementation, including the key aspects of the ground motion models, the characterization of model uncertainties, the logic-tree weights, and the sensitivity analysis and results. Finally, we critically compare the outcomes of our model both with those obtained in EMME14 and with those proposed in the national seismic design code of Iran.

2. An Overview Of The Study Area

Isfahan is located in central Iran with a centroid at the approximate coordinates of 32°38'41"N 51°40'03"E. Isfahan has an urban area of 551 km^2 and an average altitude of 1,574m. Figure 1a shows its location on the map of Iran while Fig. 1b shows the extents of its urban area. The Isfahan municipal is the third most populous city of Iran with a population of more than two millions according to the 2016 Census results published by the Statistical Center of Iran. In this section we provide a summary of the geological and geotechnical properties of the study area.

The Iranian plateau is located between the Arabian Plate in the southeast, and the Eurasian Plate in the northwest making part of the Alpine-Himalayan orogenic belt (Berberian and King 1981). This belt is seismically active with a unique pattern of deformation. Figure 1a shows also as an overview of the tectonic map of Iran. Our study area is mostly located in the central metamorphic *Sanandaj-Sirjan* zone and also partially in the *high Zagros belt*, *Zagros simply folded belt*, *Urumieh-Dokhtar magmatic assemblage* and *Central Iran*. In a more general classification, considering similarities of sedimentary facies and structures, the Sanandaj-Sirjan zone and the Urmieh-Dokhtar magmatic assemblage can be considered as part of the Central Iran zone.

The quasi-rigid Sanandaj-Sirjan zone is result of a polyphase deformation that happened in the greenschist and amphibolite metamorphic facies. This deformation is most strongly tectonized in the Zagros orogeny (Mohajjel and Fergusson 2000; Şengör 1990). Both southern and northern parts of the Sanandaj-Sirjan zone is made of rocks. While the former is most probably metamorphosed in the Middle to Late Triassic, the latter is deformed during the Late Cretaceous and therefore it contains many intrusive felsic rocks (Eftekharnejad 1981; Ghasemi and Talbot 2006; Safaei 2009). Even though in this zone the seismic activity has been relatively low in recent years, reports about the occurrence of several historical events indicate that it can be considered as an active

zone (Ambraseys and Melville 1982). The *High Zagros belt* is located between the Main Zagros Thrust and the Main Recent Fault while the *Zagros simply folded belt* is located between the Main Recent Fault and Mountain Front Fault. Most of the seismicity in Zagros is due to thrust faulting (Hassanpour et al. 2018; Jackson et al. 1995). Finally, the Urumieh-Dokhtar magmatic assemblage contains various intrusive and extrusive rocks along the active margin of the Iranian plates (Alavi 1994; Berberian and King 1981).

Based on the Global Positioning System data, deformation rates ranging from less than 2.0 mm/year in Central Iran up to around 20 mm/year in the Makran subduction zone are reported in previous studies (Khorrami et al. 2019; Vernant et al. 2004). Due to the pressures generated by this movement, large magnitude earthquakes can occur in this region. The low deformation rates in the central Iran cannot imply that large earthquakes are not probable in this region. along these lines, Craig et al. (2016) argued that "*the tectonically stable continental lithosphere can store elastic strain on long timescales, the release of which may be triggered by rapid, local transient stress changes caused by surface mass redistribution, resulting in the occurrence of intermittent intraplate earthquakes*". In fact, based on the historical records, the earthquakes of Central Iran are expected to be large albeit with long interarrival times. This further highlights the fact that the failure to record large earthquakes along the identified faults in this region cannot indicate that these faults are inactive. The 1978 M7.4 earthquake in Tabas and the 2003 M6.6 earthquake in Bam with death tolls of 15–25 and 30–50 thousands, respectively, are two examples of such events in the recent years. The absence of any earthquake records around Tabas in about 800 years prior to the large event had resulted in an erroneous belief that the region was quiet (Berberian 1979); while in Bam, no historical earthquake had been reported before the large 2003 event. As such, as suggested by Berberian (2005) and also followed in the current study, more local investigations to identify the active faults in the Central Iran crust can massively help to understand the tectonic of the region.

(a) (b)

Figure 1. (a) Summary of tectonic map of Iran adapted from Safaei et al. (2012). According to this map, the study area is mostly located in the North Sanandaj-Sirjan zone, in the South Sanadaj-Sirjan and partially in the high Zagros belt, Zagros simply folded belt, Urumieh-Dokhtar magmatic assemblage and Central Iran (*Note: the red circle indicates 200 km distance from Isfahan*); (b) Geotechnical setting of Isfahan showing the boundaries of the soil types, topography, and the location and type of the available geotechnical test data.

The geotechnical setting of Isfahan is investigated in several studies (Abdolahi et al. 2014; Ajalloeian and Jami 2010; Farashi and Ajalloeian 2012; Mohammadi et al. 2020). Herein, together with the past studies, we used the results of 369 geotechnical investigations based on standard penetration tests, SPT (303), stratigraphic logs (13) and Vs_{30} measurements (52) to identify the geotechnical setting of the study area. Figure 1b shows the location and type of the available geotechnical test data. These resources show that a major part of Isfahan is located on Quaternary alluvial sediments while small areas in the southern border and north western (i.e., areas closer to the hills) are built on the Jurassic rock units. The bedrock consists of alternating layers of "shale" and "sandstone". The alluvial sediments are composed of two distinct parts of "flood plain deposits" and "fluvial deposits" and in depth they could be distinguished by three layers of surface fine-grained, middle-coarse and lower fine-grained sediments. The predominant texture of these sediments is clay and mud. The alluvial sediments start with a small thickness in the south of the Zayandehrud River (see Fig. 1b) and the thickness increases by moving towards the north. The internal friction angle and cohesion of the alluvial sediments range between 30°–40° and 0.1–0.2 kg/cm^2, respectively, with an average elasticity modulus of 250–850 kg/cm^2.

In this study we use Vs_{30} as a proxy to account for the effects of the local soil conditions on the ground motion intensity at the surface. As such, to estimate Vs_{30} for the study area we used an hybrid approach based on two resources: (i) available geotechnical test data, and (ii) an approximate method based on the *topographical slope* proposed by Wald and Allen (2007). Given that the test data does not cover the entire area, we give more weights to the tests where they are available while the slope-based data are only used to fill in the spatial gaps. More details about the procedure used in developing the Vs_{30} map is described in the supplementary material of this manuscript. The Standard 2800 (ICSRDB 2014) Iranian national design code specifies four different soil types based on Vs_{30} values, namely Type I: $Vs_{30} > 750$ m/s; Type II: $Vs_{30} = 375–750$ m/s; Type III: $Vs_{30} = 175–375$ m/s; and Type IV: $Vs_{30} < 175$ m/s. Figure 1b shows the spatial distribution of the soil types based on this soil classification. According to this map, soil Type III is predominant (about 68% of the total area of interest) in the northern and central regions, while the southern part mainly consists of soil Type II (corresponding to about 32% of the area).

3. Datasets

3.1. Active faults

In order to provide sources for active fault-based PSHA, a new dataset of active faults for Isfahan is created herein considering a region within 200 km of Isfahan. Analysis of satellite data (Landsat ETM$^+$ and Aster) and images of geographic browser (Google Earth and Sasplanet) followed by field studies allowed us the recognition of many previously unmapped faults. As a result, a raw database including the characteristics of 125 faults is generated and further processed. It should be noted that in absence of extensive trenching and excavation data, we could not precisely determine all the features of these faults, still based on remote sensing, aerial geophysical data processing, field surveys in previous studies (Beygi et al. 2016; Safaei 2009; Safaei et al. 2012) as well as experts' judgments, we parameterized the faults to the extent possible.

Given the dextral transpression tectonics of the region, we expect to develop and extend the faults with different mechanisms such as riedel shears faults, antithetic faults, synthetic faults and tension faults which are well identified in the region. Other structures expected in transpression environments are the positive flower structure or upward-diverging faults (Fossen 2010). In this structure, when a main basement fault reaches near the ground, it turns into several parallel faults with the same mechanism. As a result of this structure, several parallel fault traces can be seen on the surface, while at depth, they merge into single main fault. In our study area, a flower structure is well observed and a large number of faults with northwest-southeast direction with this structure are identified. Based on these premises, we grouped the faults into three classes that reflect their level of importance and activity. In this process, only one representative fault is selected for a flower structure and the faults with short lengths or those where no ground motion recording could be associated to them are classified as class 2 or 3. Note that in our PSHA study, we used only the most important class 1 faults. A full map and list of all identified faults is available in the supplementary material of this manuscript.

Figure 2 shows the extent of the study area. Figure 2b shows the traces of the 23 faults classified in the fault 1 class while Table 1 lists more information about each fault. This Figure also shows the faulting mechanisms including Strike Slip (SS), Normal (N) and Thrust (T) together with the location and the event year of the main historical and instrumental earthquakes with $M_w \geq 5.0$. The final database includes fault attributes in terms of fault trace describing the geometry, kinematics, slip rate, and the associated epistemic uncertainties. Note that the slip rates were estimated based on expert judgment of the geodetic and seismic data, as well as on considerations of geomorphic expression and similar but better studied faults in the region, even if no published rates were available. For the faults lying within the quasi-rigid Sanandaj-Sirjan zone, the slip rate values are kept as low as 1.0 mm/yr in accordance with those of faults in other *stable continental regions* in the world, such as central and eastern North America (CENA) and Australia (Allen 2020; Calais et al. 2016). For faults located in the Zagros fold and Central Iran, we assumed instead an average slip rate of 2.0 mm/yr (Alipoor et al. 2012; Jamali and Hessami 2011; Khodaverdian et al. 2015; Walpersdorf et al. 2014). We emphasize that, for a more precise modeling of the faults, an extensive study to better estimate the slip velocity measurements of the new faults introduced within this study is strongly recommended in future updates of this model.

For each fault, a distribution of maximum possible magnitude (M_{max}) is calculated based on its identified features. M_{max} estimation along a fault segment has been a topic of discussion for many years (Mignan et al. 2015; Zöller et al. 2013). Herein, we consider multiple approaches to estimate the values of M_{max}: (i) based on the maximum observed magnitude along the fault (M_{max}^{obs}), (ii) as a function of the seismic moment, $M_{max}^{M_0}$ (Hanks and Kanamori 1979) ; and, (iii) based on the fault's capacity using the empirical relationships, M_{max}^{cap} (Leonard 2010; Leonard 2014; Nowroozi 1985; Wells and Coppersmith 1994), which are a function of the fault's physical parameters, such as surface fault length, subsurface fault length, down-dip fault width, fault area and average displacement per event. Table 1 lists a summary of the calculations based on different methods. For defining the final distribution of M_{max} (M_{max}^{final}), we used the Monte Carlo method using the distributions of $M_{max}^{M_0}$ and M_{max}^{cap} based on different references while we used the M_{max}^{obs} as the minimum threshold value.

Table 1
Fault database including the name, mechanism, average strike, DIP and rake angles along the faults trace, the slip velocity and estimated M_{max} of each fault.

No	Fault Name	Fault Mec. ▯	Strike (°)	DIP (°)	Rake (°)	Slip Rate ($mmyr^{-1}$)	M_{max}^{obs}(year)	$M_{max}^{M_0}$§		M_{max}^{cap}		M_{max}^{final}	
								$\bar{m}$	σ	$\bar{m}$	σ	$\bar{m}$	σ
1	Meymeh	SS	155	45 NE	135	1.0	4.0 (2000)	6.9	0.27	7.5	0.2	7.4	0.36
2	Soh	N	0	60 E	-135	1.0	6.4 (1844)	6.8	0.28	7.5	0.3	7.3	0.41
3	Hanjan	N	100	60 E	-135	1.0	3.2 (2006)	6.7	0.28	7.3	0.3	7.2	0.39
4	Kashan	T	120	50 SW	135	2.0	5.8 (1778)	7.4	0.19	8.0	0.2	7.9	0.35
5	Hasanrobat	T	125	50 SW	135	1.0	6.4 (1880)	6.9	0.26	7.5	0.2	7.4	0.35
6	Khomeynishahr	N	0	50 E	-105	1.0	3.9 (2004)	6.7	0.29	7.3	0.3	7.2	0.39
7	Gavart	N	130	55 W	-135	1.0	4.1 (2013)	6.6	0.28	7.4	0.3	7.2	0.42
8	Tiran	T	125	45 SW	120	1.0	4.4 (1992)	7.3	0.22	8.0	0.2	7.8	0.35
9	Pirbakran	T	145	45 NE	130	1.0	4.2 (2005)	7.0	0.24	7.6	0.2	7.5	0.35
10	Dina	N	170	55 NE	-115	2.0	5.3 (2018)	7.2	0.22	7.8	0.2	7.7	0.36
11	Hafshejan	T	130	45 NE	135	2.0	6.4 (1868)	7.4	0.21	8.0	0.2	7.8	0.36
12	Dehshir	T	155	45 NE	120	2.0	3.5 (2019)	7.3	0.22	7.9	0.2	7.8	0.35
13	Semirom	T	145	45 NE	135	2.0	6.6 (1459)	7.3	0.23	7.9	0.2	7.7	0.36
14	Siasakht	T	145	45 NE	135	1.0	6.8 (1874)	7.4	0.22	8.0	0.3	7.9	0.37
15	Baghmalek	N	165	60 NE	-135	1.0	6.2 (1978)	7.0	0.29	7.6	0.2	7.4	0.37
16	Farsan	T	140	45 NE	135	1.0	7.3 (1909)	7.1	0.25	7.8	0.2	7.6	0.36
17	Sahlabad	T	140	50 SW	135	1.0	4.4 (2012)	7.0	0.26	7.6	0.2	7.5	0.36
18	Verjan	T	120	45 SW	135	1.0	4.7 (2013)	7.0	0.27	7.7	0.2	7.5	0.36
19	Maranjab	T	85	45 S	65	1.0	4.1 (2006)	6.6	0.28	7.3	0.2	7.1	0.39
20	SefidShahr	N	65	60 SE	-45	1.0	3.9 (2002)	6.6	0.29	7.3	0.3	7.1	0.43
21	Kuh-e-Latif	T	100	40 N	65	0.5	4.4 (2000)	6.7	0.27	7.3	0.3	7.1	0.40
22	Garab	T	140	45 SW	115	1.0	5.6 (1939)	6.9	0.28	7.6	0.2	7.4	0.37
23	Kuh-e-Bababozorgi	T	85	45 N	45	0.5	4.4 (2000)	6.6	0.28	7.2	0.2	7.1	0.38

▯ Fault mechanism: SS: Strike Slip; N: Normal; T: Thrust

§ $M_{max}^{M_0} = \frac{2}{3}(\log_{10}M_0 - 9.1)$; $M_0 = \mu LWD$; where μ is the shear modulus (herein assumed to be ~ 3.0×10^{10} Pa); L is the fault rupture length and W is the down-dip width and D is the average slip on the fault.

3.2. Earthquake catalogue

PSHA commonly starts with assembling a complete (in space and time) earthquake catalogue of events characterized by a homogeneous magnitude definition. The catalogue is required for proper definition of the past earthquake occurrences (and for forecasting future ones) and is the basis for the development of area seismic source recurrence characteristics and for performing smoothed seismicity analyses. Earthquake catalogues typically consist of an historical part, which summarizes historical reports on observations of earthquakes occurred in the distant past, and an instrumental part related to the recent seismicity detected by seismic networks. In the following, we provide a description of the catalogue resources and harmonization of the earthquake magnitude. Table 2 lists the sources of the catalogues as well as the covered year and magnitude range. Figure 3 shows the spatial distribution of the events and their moment magnitudes.

Table 2
Catalogue resources. The values correspond to the events occurred in a rectangle within 48°E– 54°E and 29°N–36°N. Legend: MMI = Modified Mercali Intensity; Mn = Nuttli magnitude; m_b=body wave magnitude; M_l= local magnitude; M_s,= surface magnitude.

Catalogue	Covered period	Magnitude Range (M_w)	Magnitude Types	No. events
Historical	1052–1880	5.9–6.8	MMI	17
ISC	2006–2020	2.5–4.3	M_N	10100
IIEES	1909–2006	1.5–7.3	m_b, M_s, M_l	1320

Ambraseys and Melville (1982) collected information about the historical earthquakes in Iran, originally based on chronicles of historical manuscripts. Herein, we identified 17 historical events that are reported in terms of macroseismic intensity (MMI) within the study region. The instrumental catalogue obtained from two sources, ISC and IIEES, consists of events that can affect the study area and it spans between 29.0°N–36.0°N and 48.0°E–55.0°E. ISC is a more complete database than IIEES, it provides more precise coordinates of the epicenters but is only available from 2006 to date. As such, we compiled the instrumental catalogue using the IIEES database in the interval of 1909–2005 and using the ISC database for the interval of 2006–2020. The entire catalogue was then harmonized to moment magnitude. Table 3 shows the list of the conversion relationships used in this study. For the historical events, we considered a two-step process that converts the MMI to surface magnitude (M_s) through the conversion equations proposed by Papadopoulos et al. (2014) and from M_s to moment magnitude (M_w) using the conversion relations of Scordilis (2006). IIEES reports magnitudes in terms of body wave magnitude, m_b, surface magnitude, M_s, and local magnitude, M_l, while ISC is based on Nuttli magnitude (M_N). All different magnitude types are converted to M_w using the equation of Scordilis (2006) for m_b and M_s, that of Zare et al. (2014) for M_l, and that of Sonley and Atkinson (2005) for M_N.

The instrumental catalogue includes mainshocks as well as clustered events, also referred to as foreshocks and aftershocks. Assuming a Poissonian recurrence of the earthquakes in terms of location and magnitude, typically only mainshocks are used to assess the recurrence parameters in a time-independent seismic hazard assessment (Frankel 1995). Therefore, conforming to this assumption, herein we removed the clustered events from the instrumental catalogue using the Gardner and Knopoff (1974) declustering algorithm. The declustered instrumental catalogue is left with 3,439 out of the 11,416 events spanning the magnitude range of M_w=2.0–7.3 contained in the original catalog. Note that, although the choice of different methods, such as the declustering algorithm or the homogenization of the catalogue, may affect the final PSHA results (Beauval et al. 2020), such impacts are not investigated here. We assume that the adopted approaches represent a central path.

Table 3
Relationship between M_s, M_l, m_b, M_N and M_w used in this study

Magnitude Type	Conversion relation	Boundary	Source
I_m, M_s	M_s=(4.12471 ± 0.25587)+(0.24996 ± 0.0328)I_m	$I \leq I_m \leq$XII	Papadopoulos et al. (2014)
m_b, M_w	M_w=0.85(± 0.04)m_b+1.03(± 0.23)	$3.5 \leq m_b \leq 6.2$	Scordilis (2006)
M_s, M_w	M_w=0.67(± 0.005)M_s ±2.07(± 0.003)	$3.0 \leq M_s \leq 6.1$	Scordilis (2006)
	M_w=0.99(± 0.002)M_s ±0.08(± 0.13)	$6.2 \leq M_s \leq 8.2$	
M_l, M_w	M_w=*1.0136M_l − 0.0502*	$4.0 \leq M_l \leq 8.3$	Zare et al. (2014)
M_N, M_w	M_w=*1.03M_N − 0.61*	$1.0 \leq M_N \leq 6.0$	Sonley and Atkinson (2005)

4. Seismic Source Characterization

As alluded earlier, we generate a source model consisting of a combination of two components based on distributed seismicity and finite faults. The former stands on the analysis of the harmonized earthquake catalogue, while the latter uses the database of available slip rates from geologic and geodetic observations. Both models have pros and cons. While the distributed seismicity model is well calibrated to account for spatial variability of the earthquake process, the faults model better constrains the long recurrence interval earthquakes and the localized seismicity around the known major tectonic structures. As such, we intend to compensate their limitations through a reasonable combination of both. In the following sub-sections, we briefly discuss the main characteristics of the two source models.

4.1. Seismic source zonation, occurrence model and M_{max}

Seismic source zones (SSZs) are the geographic regions that are delineated on the basis of geological, geophysical, and/or seismological similarities (Reiter 1992). SSZs are basically geographic polygons of assumed uniform seismicity. In addition, the maximum magnitude, depth, style of faulting, strike, dip and rake are assumed spatially invariable within a zone. Herein, we follow the prescriptions of Vilanova et al. (2014) for the definition of the zones. Our zonation is mainly based on (i) the analysis of the earthquake catalogue in terms of completeness intervals, seismic activity rates and seismogenic depths; and, (ii) the surface geometry of the faults and the geological settings as well as style of faulting. Based on this concept, we discretize the study area into seven independent source zones, Z1 to Z7. In this zonation process, we have assured the compatibility with the EMME seismogenic source model (Danciu et al. 2017; Şeşetyan et al. 2018) and the geological zonation studies of Iran (Arian 2015; Nogole-Sadat and Almasian 1993; Oveisi et al. 2019).

Figure 3 shows the extents of the zones and the spatial distribution of the events within each zone. Z1 and Z3 lie within a tectonic environment that is adjacent to major plate boundaries. However, they have not generally undergone any recent large tectonic deformations or large earthquakes and, thus, they can be classified as *stable continental* (Calais et al. 2016; Johnston et al. 1994). Z3 basically lies within the Sanandaj-Sirjan zone and, as described earlier,

despite the few events in this region with no events of $M_w \geq 5.0$, it cannot be considered inactive. For instance, within this study multiple active faults are identified in Z3 albeit with lower slip rates than those of faults in other active regions, such as Zagros (i.e., zone Z2). Therefore, characterizing these regions only based on the observations and background seismicity may result in an underestimation of the seismic hazard. We compensate this limitation by a thoughtful considerations on the choice of M_{max} (Calais et al. 2016) and by relying on the fault source models for generation of long recurrence interval large magnitude events. A more detailed discussion on this aspect is provided in the following sections of this manuscript.

On the other hand, as can be seen in Fig. 3, the earthquake productivity in the active zone of Zagros (i.e., Zone Z2) is significantly larger with 62 events with $M_w \geq 5.0$ observed in this zone. Zones Z4, Z5 and Z6 are delineated in order to lie within Urumieh-Dokhtar, Alborz, and Central-Iran geological zones, respectively. Note that Z2, Z4, Z5 and Z6 are classified as *active shallow crustal* regions. In the characterization of zones Z1–Z6, we have considered all the events with hypocentral depth of less than 50 km. Figure 3b, which shows the spatial distribution of events' depths, shows that most of the deep events (with hypocentral depth ≥ 50 km) are concentrated beneath the Zagros fold. According to the geological studies, this region consists of mainly carbonate and marly facies, i.e., early Cretaceous (Nogole-Sadat and Almasian 1993). As such, zone Z7, which lies partially within Z2, is also considered to represent the *deep seismicity* region of Zagros. It should be noted that Z1 lies outside of the 200 km distance from the center of Isfahan and the events in this zone may have negligible impact on its urban area of Isfahan. Nevertheless, the contribution to the hazard from Z1 is also reported here for the sake of completeness.

For each one of the seven zones we derived a doubly truncated Gutenberg-Richter (GR) relation from the declustered catalogue following a completeness analysis based on the method of Stepp (1972). For each zone, the *a*-value (a^{GR}) and *b*-value (b^{GR}) of the GR relation were then calculated using the maximum likelihood estimation method that considers unequal completeness intervals for different magnitude ranges using the Weichert (1980) algorithm. To achieve a good fit with the data, in the completeness analysis of the catalog we have considered multiple magnitude thresholds (i.e., M_{lower}^{GR}) and magnitude bins. These parameters are iteratively adjusted to provide the best solution of the GR relation and, as such, they vary between zones. Note that when performing the hazard calculations, a common minimum magnitude threshold of $M_{\min}$=4.0 has been considered for all zones, assuming that this is the lowest magnitude that is capable of causing damages to the structures in the urban area of Isfahan. With a seismic risk analysis perspective, Bommer and Crowley (2017) defined $M_{\min}$ as the lower value of the earthquake magnitudes that, if reduced, does not result in higher risk estimates even though it may result in higher seismic hazard estimates. For more clarifications on the choice of this parameter a sensitivity analysis is presented towards the end of this manuscript.

The estimation of the maximum magnitude in PSHA is a complex, and often controversial, aspect that should be guided by information from geology and the seismotectonic of a seismic source. Herein, for definition of M_{max} for each zone, we considered three approaches including: (i) the maximum observed event within the zone (M_{obs}) plus 0.5 unit (M_{max}^{obs}); (ii) the non-parametric Gaussian method of Kijko (2004), M_{max}^{Kijko}; and, (iii) the estimated maximum magnitude that the faults within the zone are capable of generating, M_{max}^{fault} (see Sect. 3.2 and Table 1). Based on these three estimates, the maximum value is selected as the M_{max} of the zone. However, to account for the uncertainty on this value, we considered different models with M_{max}±0.2 in the logic tree adopted in the PSHA. Further discussions on the structure of the logic tree are provided in Sect. 6.

Figure 4 shows the GR fit for each zone in comparison with the observed data. This figure also shows different trials of the M_{lower}^{GR} and the corresponding obtained b^{GR} values and the different realizations of the selected branch (grey lines). Table 4 provides a summary of the results of the zonation analysis and also compares the corresponding GR parameters and M_{max} values that were adopted in EMME. Note that the delineation of the zones in this study is different than that in EMME14 and, thus, we could only approximately extract the GR parameters from EMME14 using the definition of normalized (to area) a^{GR}. Nonetheless, this comparison provides us with an understanding of the likely differences between the two studies. For instance, because EMME is based on a regional model and the seismic super zones cover larger areas, in general the distributed productivity rates in EMME are larger than those estimated in this study.

No	Tectonic Region†	Events No. §		This study			
				a^{GR}	b^{GR}	M_{max}	M_{max}^{obs} ††
SC		79	3.61	0.98	3.30	**5.1** ▯	4.9
Z2	ASC		1201	3.99	0.81	3.00	7.8
Z3	SC		131	3.13	0.78	3.00	6.2
Z4	ASC		147	3.63	0.95	3.00	6.9
Z5	ASC		220	4.19	1.03	3.00	**6.4**
Z6	ASC		247	4.33	1.06	3.20	6.3
Z7	DS		118	3.51	1.06	3.20	6.2

† SC: Stable Continental; ASC: Active Shallow Crust; DS: Deep Seismicity

§ Note that these are the number of events within each zone with $M_w \geq 3.0$

▯ Bold M_{max} values in the table are the selected mean M_{max} values for the zone.

†† M_{max}^{obs} is the maximum observed magnitude within the area (M_{obs}) plus 0.5 unit of magnitude.

We analyzed the depth of the events from the catalogue within each zone to characterize the hypocentral depth distribution in hazard calculations. Figure 5 shows the normalized histogram (i.e., probability of being in the interval) of the event depth for each zone. We considered five depth intervals for zones Z1 to Z6 and four depth intervals for Z7 that range between 0–50 km and 50–140 km, respectively. These probability values are then utilized in the source modeling. It should be noted that to make a realistic statistic of the data, we have eliminated the depth values of 0, 5, 10 and 33 km from the database, assuming that when no information was available, such round numbers were inserted in the database. With reference to Fig. 5, most of the events in Z1 to Z6 had an hypocentral depth in the bins of [0, 10] km and [10, 20] km, while in zone Z7, the hypocentral depths are mainly spread in the bin of [50, 70] km and [70, 90] km with a negligible percentage of events occurred deeper.

Note that we found more than 160 events deeper than 50 km in our catalogue most of which in the Zagros region (see Fig. 3b and the area in Z7), which is in contrast with the findings of several past studies (Kalaneh and Agh-Atabai 2016; Karasozen et al. 2018; Talebian and Jackson 2004). This may imply that there is a systematic error in the reported hypocentral depth of deep events of our catalogue. This topic, nonetheless, is debatable as several geological evidences are reported in previous studies (McQuarrie 2004; Sepehr and Cosgrove 2004) addressing the possibility of deep seismicity in the region, due to the differences in time and the manner of collision of plates in different parts of the Arabian and Iranian plates. Such phenomenon has clearly caused an increase in the thickness of the Iranian crust in the central parts of Zagros and thus provides an evidence for deep seismicity in zone Z7. In the delineation of Z7 we used satellite images to recognize the borders of the outcrops, which are mainly carbonate and marly facies of early Cretaceous, and to distinguish between the deep and non-deep parts of the region. Finally, as stated earlier, based on the data in our possession we decided to keep deep zones in our study, although more studies on the subject are recommended. However, given the large distance of Z7 from our study area, we do not expect a significant hazard contribution from this zone.

To account for the spatial variability of the seismicity, as described in Poggi et al. (2020), we use a smoothed seismicity approach (Frankel 1995) to redistribute the annual occurrence rates within each polygon (i.e., Z1–Z7) considering the spatial density of earthquakes using an isotropic seismicity smoothing kernel. This approach allows using zone specific b^{GR} and seismic modeling parameters such as rupture mechanism, depth distribution and M_{max}. We considered a set of spatially distributed grid points with 0.1°×0.1° spacing covering the entire area. In addition, to account for the modeling uncertainty, we used three different correlation distance values, C_d, (Frankel 1995) equal with 10, 40 and 70 km. As an illustrative example, Fig. 6 shows the cumulative annual rates (M_w>0) within the zones using C_d =10 and 70 km.

4.2. Faults and background seismicity source Modeling

In this section we describe the fault source modeling approach including the style of faulting and magnitude-frequency distribution (MFD). We herein follow the modeling approach referred to as simple fault in the OpenQuake engine (Pagani et al. 2014) which is represented by the surface projection of the fault traces with a constant dip. In absence of detailed fault information, this is an easy way to account for complexity of the fault geometry with no considerations about the changes in dip along the fault strike. We assume that each fault is bounded within the seismogenic thickness, which we herein considered in the range of 5–30 km. The spatial extent of the ruptures along the fault is defined based on the magnitude scaling relation of Wells and Coppersmith (1994) and on the rupture aspect ratio.

To characterize the seismic activity of the faults, we use model type 2 of Anderson and Luco (1983) based on a truncated exponential MFD (in agreement with the distributed seismicity model). Basically, the earthquake occurrences are defined based on the slip rates, herein inferred by geodetic considerations as listed in Table 1, given the fault expression and geometry. Note that the b^{GR} value for each fault is derived from the statistical estimates obtained from the entire

zonation study (see Table 4). In the MFD calculations for all faults we assumed a crust shear modulus of $\mu = 3.0\times10^{11}$ dyne/cm^2 and an average fault-slip to fault length ratio of $a = 1.25\times10^{-5}$. In our modeling we have assumed that the slip rate is constant across the fault area and that there is no creeping.

As shown in previous studies (Hofmann 1996; Wesnousky et al. 1983) and implemented in other urban (Ebrahimian et al. 2019) and regional (Danciu et al. 2017; Poggi et al. 2020) hazard analysis studies, modeling a unique MFD relationship for the faults for all magnitude ranges (small, moderate and large) may result in an increase of small to moderate earthquakes compared to the observations. A common practice to alleviate this problem is to use fault modeling only for the larger magnitude earthquakes and to use a background seismicity model for small to moderate events. Herein, we considered the above-described fault source modeling for magnitudes larger than a threshold value, $M_w > M_{thre}$, and a distributed seismicity model with C_d=40 km is used for $M_w \leq M_{thre}$ in the faults and background seismicity (FSBG) models. Note that to account for the epistemic uncertainty for the choice of M_{thre}, we considered three values of M_{thre}= 5.5, 6.0 and 6.5 in our source model logic tree. More details about the logic tree are provided in the following sections.

5. Ground Motion Prediction Equations

GMPEs are one of the main factors that influence the accuracy of PSHA and risk assessment results (Crowley et al. 2005). In parallel with the improvements in strong motion networks and the availability of ground-motion data, the number of GMPEs has significantly increased (Douglas and Edwards 2016). The large database of available GMPEs makes the procedure of GMPE selection a scientific challenge. In this process, several aspects of the GMPEs including the tectonic regime, the site effects modeling, regional or global database utilized for the development, and distance and magnitude applicability of the model should be accounted for to avoid arbitrary choices (Danciu et al. 2016a). For this reason, several methods have been used in the literature to evaluate the performance of GMPEs in PSHA using observed ground motions from the region of interest. These methods include residual analysis methods (Scasserra et al. 2009), likelihood, LH, and log-likelihood, LLH (Mousavi et al. 2012) methods, and Euclidean distance based ranking, EDR, methods (Kale and Akkar 2013), among others.

According to Danciu et al. (2016a), a site-specific PSHA requires the use of multiple GMPEs that can both describe the local characteristics of the ground motion database of the region and at the same time they should account for the completeness of the dataset at a large scale. Three seismotectonic regions including *active shallow crust*, *stable shallow crust* and *deep seismicity* are identified within 200 km distance from the study area. The GMPEs of ASB14 (Akkar et al. 2014), CY08 (Chiou and Youngs 2008), AC10 (Akkar and Cagnan 2010) and Zetal06 (Zhao et al. 2006) were recommended by EMME14 for active shallow crustal tectonics of the region. According to Fallah Tafti et al. (2017) and based on the EDR method CB14 (Campbell and Bozorgnia 2014), BSA14 (Boore et al. 2014), CY14 (Chiou and Youngs 2014), ASK14 (Abrahamson et al. 2014) and Zetal06 (Zhao et al. 2006) were ranked as the most appropriate GMPEs for the seismicity in Iran. Zafarani and Mousavi (2014) investigated the best fitting GMPEs for Iran based on two methods of LH and LLH. Their study supports the use of AS08 (Abrahamson and Silva 2008), CY08 and Getal09 (Ghasemi et al. 2009) based on the former method; whilst Getal09, AS08 and CY08 were ranked as the best GMPEs according to the latter one. More recently, Farajpour et al. (2020) concluded that the NGA-West GMPEs of BSA14 and ASK14 perform better for Iran. This study also showed that, among the local GMPEs, those proposed by Darzi et al. (2019) and Farajpour et al. (2019) fit well with the recorded data at the short periods, e.g., between *PGA* and *Sa*(0.2s), while for longer periods the models of Zafarani et al. (2018), Sedaghati and Pezeshk (2017) and Ketal15 (Kale et al. 2015) are preferable.

Following all these suggestions while also seeking a consensus with the aforementioned local studies for Iran, we selected the four GMPEs of Ketal15, ASB14, CY14 and Cauzzi et al. (2015) with weights of 0.30, 0.3, 0.3, 0.1, respectively, in the logic tree for active shallow crustal zones (i.e., Z2, Z4, Z5 and Z6). This choice also intends to represent the four categories of GMPEs suggested by Danciu et al. (2016a). Given the few GMPEs available in the literature for stable shallow crust and deep seismicity, we have, however, a limited number of choices. For stable shallow crust (i.e., Z1 and Z3), we considered three GMPEs of SP16 (Shahjouei and Pezeshk 2016) and PZT11 (Pezeshk et al. 2011) and AB06 (Atkinson and Boore 2007) with equal weights. These GMPEs are developed for the stable continental regions of CENA similar to those of this study. Finally, following the suggestions of EMME (Danciu et al. 2016a), we use the two GMPEs of LL08 (Lin and Lee 2008) and Yetal97 (Youngs et al. 1997) for the deep seismicity zone (i.e., Z7) with equal weights of 0.5. Figure 7 shows the trellis plots for the three GMPEs selected for stable continental region while the figures for other GMPEs are shown in the supplementary material of the manuscript.

6. Handling Uncertainties: Logic Tree

To account for the epistemic uncertainty in seismic source modelling and modeling parameters, we considered a *source model logic-tree* with four branching levels. Firstly, we generated three independent distributed seismicity models using C_d=10, 40 and 70 km. Herein, we assumed that C_d=40 km is a better representative of the spatial distribution of the events, as such we have considered a larger weight of w = 0.5 for this branch level and w = 0.25 for the other two branches. Secondly, to account for the uncertainty in b^{GR} fitting we considered three sub-branches using the mean b^{GR} and mean-b^{GR}±0.05. Similarly, in the third branching level we considered three alternative values for maximum magnitude with the mean M_{max} and mean M_{max}±0.2 of magnitude unit. For these last two branching levels we use w = 0.5 for the central values and w = 0.25 for upper and lower bounds. A fourth branching level accounts for the uncertainty in the selection of the threshold magnitude in the FSBG model whereby we considered three branches with M_{thre}=5.5, 6.0 and 6.0 with equal weights under the FSBG source model. Figure 8 shows the entire logic-tree structure, including the branching levels for both the source and the ground motion model uncertainties. Note that to account for the uncertainty on other parameters, such as DIP and rake angles in our modeling, we considered some reasonable ranges with uniform distributions around the central values.

Branches of Source modeling					Branches of GMPEs		
Source Model	C_d (km)	b^{GR}	M_{max}	M_{thre}	Stable Continental	Active Shallow	Deep Seismicity

Figure 8. Logic tree structure used in the PSHA of this study

7. Results Of The Psha

We performed hazard calculations for multiple intensity measures including *PGA* and pseudo spectral accelerations (*Sa*) at several periods on rock and soil conditions The PSHA calculations are performed using the latest available OpenQuake version 3.10.1. The calculations are performed for more than 3000 sites spread over the urban area with a grid spacing of approximately 500×500 m. The results of the PSHA are computed for both the reference rock conditions of Vs_{30} = 800 m/s and also accounting for the soil conditions via the Vs_{30} discussed in Sect. 2 and Figure S5 shown in the supplementary material of this manuscript. Here we present some of the selected results in terms of hazard curves, disaggregation analysis, hazard maps and uniform hazard spectra (UHS). Figure 12 shows the mean and different percentiles of the hazard curves for *PGA*, *Sa*(0.3) and *Sa*(1.0) for a selected site while Fig. 12 shows the results of the disaggregation analysis (Bazzurro and Cornell 1999) for *PGA* corresponding to 475 and 2,475 years return periods (T_r).

Figure 11. Mean hazard maps of *PGA* [g] on reference rock (Vs_{30} = 800 m/s) corresponding to the hazard level characterized by 10% probability of exceedance in 50 years (T_r=475) based on: (a) combined source model; (b) faults and background seismicity model; and, (c) distributed seismicity model.

T_r = 100 years	T_r = 475 years	T_r = 975 years

Figure 12. Mean hazard maps of *Sa*(0.3s), *Sa*(0.75s) and *Sa*(1.5s) [g] on soil corresponding to different hazard levels: **Left column**: 39% probability of exceedance in 50 years (T_r=100); **Middle column**: 10% probability of exceedance in 50 years (T_r=475); **Right column**: 5% probability of exceedance in 50 years (T_r=975).

Figure 13 compares the PSHA estimates in terms of Uniform Hazard Spectra (UHS) from this study, and from EMME14 with the design spectra from the Standard 2800 code for soil types 2 and 3. Note that in this Figure the UHS are based on the 475 and 2,475 years hazard levels. Note that the T_r=475 years is assumed to be the basis for the design spectrum of Standard 2800 (Kohrangi et al. 2018). For comparison purposes, this Figure shows the mean, 10th and 90th percentiles of the UHS. Note that UHS shown in Fig. 13 for a given soil type are the mean of the UHS of all sites classified in that soil category in the urban area of Isfahan. According to Standard 2800, the reference 475 years *PGA* on bedrock for Isfahan is A = 0.25g (where g is the acceleration of the gravity) whereas according to Fig. 12a, the *PGA* on reference rock (vs30=…) obtained from the PSHA ranges between 0.16–0.22g. With reference to Fig. 13, for sites with soil type 2 and 3, the mean UHS ordinates derived herein are lower but, overall, reasonably match those derived from EMME14 for spectral ordinates higher than 0.50s at both return periods. On the other hand, the design spectrum, which is significantly higher even than the 90th percentile of the 475 year UHS from this study and of the mean UHS of EMME14, provides conservative spectral values for all spectral ordinates.

8. Sensitivity Analysis

Among other crucial steps to conduct and document a complete site-specific PSHA study (Budnitz et al. 1997), a fundamental one is a sensitivity analysis which helps to quantify whether the range of epistemic uncertainties in the PSHA modeling is properly captured by the logic tree. Herein, we performed a sensitivity analysis to investigate the effect of our modeling assumptions in the definition of the source model and GMPEs branches included in the PSHA logic tree. These assumptions include the values of the parameters such as b^{GR}, M_{min}, M_{max}, C_d, threshold magnitude in the FSBG model, $M_{threshold}$.

Figure 14 shows a comparison of the UHS obtained via some of the selected individual branches of the logic tree. In Fig. 14a, the grey lines show the mean UHS for different branches of the source model while the mean, 10th and 90th percentiles of UHS are shown in blue. Figure 14a also shows the UHS obtained from the combination of the EMME source model with the GMPE branches of this study. Similarly, the grey lines in Fig. 14b show the mean UHS using the source model logic tree of this study but for different individual branches of the GMPE utilized in the logic tree. In other words, for each realization of Fig. 14b we used only one GMPE of each branching level (e.g., one individual branch is a combination of AB06, Ketal15 and LL08d for “stable continental’, “active Shallow crustal” and “Deep Seismicity”, respectively) to compute the UHS. In this Figure we also compare the results with the mean UHS obtained from the combination of the EMME14 GMPE branches with the source model of the current study. This comparison shows the high sensitivity of the hazard estimates stemming from the GMPE selection (Fig. 14a), which conforms the statement in (Crowley et al. 2005), while the source models of EMME and this study (although created based on different data and assumptions and techniques) do not introduce significant discrepancies in the mean UHS estimates (Fig. 14b).

A more quantitative comparison on the impact on hazard estimates of different values of the modeling parameters is shown in Fig. 15. This Figure shows for a selected site with rock conditions, the percentage difference among the mean estimates of *PGA* and *Sa*(1.0s) for T_r=475 and 2,475 years obtained from single branches of the source model and those from the full source model adopted in the logic tree of this study. For T_r=475 years, the b^{GR}±0.05 and M_{max}±0.2 have an impact of about ± 10%, while for T_r=2,475 the impact increases up to about ± 20%. Similarly we observe a significant impact of M_{thre} of up to + 30% for T_r=2,475 years when M_{thre}=5.5 is used. However, the impact of M_{thre} for shorter return period and for other magnitude threshold values is between ± 15%. The selection of C_d apparently shows a relatively higher impact as the upper and lower bound C_d of 10 km and 70 km cause a maximum difference of − 30% and 20%, respectively. In addition to the variations in the values included in the logic tree, to augment the breadth of the sensitivity analysis we also considered running the model for different assumptions of M_{min}, i.e., M_{min} =4.5 and 5.0 instead of the originally adopted value M_{min}=4.0, and for different variations of the weights assigned to the source models, namely “50% FSBG + 50% Distributed seismicity” and 100 % FSBG versus 100% distributed seismicity. Using a higher M_{min} value, as expected, reduces the number of events and thus reduces the hazard estimates by approximately 10–35%, while different weighing of the FSBG and distributed seismicity models generate smaller differences between ± 10%.

Note that while the definition of our logic tree was basically guided by our sensitivity analysis, the final selected logic tree of our study is based on educated decisions made by the authors. Therefore, another group of researchers starting from the same raw datasets may very well end up with a materially different logic tree definition and weights. Nevertheless, with reference to our observations in this sensitivity analysis, we can claim that we have successfully captured the central value of all different variations in the modeling parameters, critical assumptions and weighting procedure considered in the logic tree.

9. Summary And Concluding Remarks

We performed a probabilistic seismic hazard analysis (PSHA) for the urban area of Isfahan (central Iran). We carried out a detailed source characterization for PSHA using the most recent catalog of historical and instrumental earthquakes and an original database of seismogenic sources produced by this study. Our seismogenic source comprises of 23 individual parametrized active faults identified within 200 km radius from the urban area. Based on these two datasets, we developed two seismogenic source models including (i) a distributed seismicity model; and, (ii) a faults and background seismicity model. The study area is sub-divided into seven distinct zones with distinguished geological and seismicity characteristics. We then classified these seven zones into the three tectonic regions of *active shallow crust*, *stable continental* and *deep seismicity* regions. To efficiently account for the spatial distribution of the events within the distributed seismicity model, we considered a smoothing occurrence rate redistribution following the recommendations of Poggi et al. (2020). For each seismotectonic region, we selected a group of most recent ground motion prediction equations (GMPEs) to quantify the ground motion intensity on rock and soil conditions. The effects of local soil conditions is accounted for through $Vs_{30,}$ which is as a proxy variable available in all of the GMPEs selected in this study. The Vs_{30} values in Isfahan were estimated based on the available geotechnical test data and the slope-based Vs_{30} values. Finally, we accounted for the uncertainty in the source modeling assumptions and ground motion intensity characterization via a logic tree approach.

We implemented the source model in OpenQuake and performed PSHA for a number of intensity measures including *PGA* and pseudo spectral accelerations for oscillator periods ranging from … to... We then generated hazard maps and uniform hazard spectra (UHS) for multiple intensity levels corresponding to 100, 475 and 975 years return periods. We compared the seismic hazard results obtained in this study with the results of the regional earthquake model for Middle East (EMME) and the seismic design spectrum of the Iranian national design code. The results of our model are lower but generally in good agreement with those of EMME14 especially for the spectral ordinates larger than 0.5s. This difference can be due to multiple aspects including the definition of the new fault model developed in this study, dissimilarities in both the seismogenic source delineations and the GMPEs adopted in the two studies.

The comparison of 475 year UHS of this study with the seismic design spectrum of the Iranian code shows that the latter is significantly higher than the former and, therefore, we can speculate that the design code is quite conservative. Although certain level of conservatism for low seismicity regions is understandable and somewhat expected in design codes, this level of conservativism could perhaps be transparently acknowledged so that the end users could better gauge the level of safety achieved by the structures they design using the code. Two alternative ways to do so could involve in low to moderate seismicity regions either prescribing to design for ground motions with return periods longer than 475 years, as is done in ASCE7 (2016) for CENA, or by adopting for design a percentile of the at 475 year ground motion intensity (e.g., 84th percentile) higher than the median or the mean (Abrahamson and Bommer 2005). One such modifications seem necessary for many sites in Iran especially those located in the Sanandaj-Sirjan region where the so called stable continental region of Iran is located.

Although to our knowledge this study provides the most comprehensive PSHA done for the city of Isfahan to date, we emphasize that it could be further enriched and updated by considering multiple aspects. First, a thorough study as well as field investigations are essential to better characterize the fault database in terms of their slip rates and their geometry. On the other hand, Isfahan is mainly located on a stable continental region (i.e., Zone Z3 of this study) and even though using faults as seismic sources in the PSHA model is in our opinion highly recommended, whenever possible, such an approach requires caution and attention. In such quasi-rigid zones, steady displacements are rather low and thus accounting for large events with long interarrival times in stable continental via fault modeling has been debated in the community. This is indeed an ongoing research topic (Calais et al. 2016) but dwelling on such a matter is beyond the practical scopes of this study. Second, in the current study we used Vs_{30} as a proxy to account for the effects of local soil conditions on PSHA estimates at the surface. Although what was done here is the traditional approach, if better geotechnical data were to become available more precise analyses could be adopted to account in the PSHA for the amplification factors as well as their uncertainty at any given site (Bazzurro and Cornell 2004; Rodriguez-Marek et al. 2014) of Isfahan urban area.

Declarations

Acknowledgements

Our work was partially supported by Project “Seismic micro-zonation of Isfahan urban area” funded by the municipality of Isfahan under contract number 98/8059. This support is gratefully acknowledged. Any opinions and findings expressed in this manuscript are those of the authors and do not necessarily reflect those of the sponsor. We thank the Isfahan Urban railway organization, Minister of roads and urban development of Isfahan as well as Isfahan construction engineering organization for providing us with the geotechnical reports for Isfahan used in generation of the hybrid Vs_{30} map. The first author is thankful to Dr. Hamid Zafarani for fruitful discussions regarding the technical aspects of the model. Finally, we acknowledge the technical supports of Dr. Somayeh Farashi, Eng. Nasrin Jami and Dr. Mojtaba Heidari from Isfahan Department of geology for their help in generation of the Vs_{30} database which was then used to develop the Vs_{30} map.

References

Abdolahi M, Jafarian M, Goodarzi G, Pirhadi G, Partoazar H (2014) Geology map reports for Isfahan-Felavarjan. Geological Survey & Mineral Explorations of Iran (GSI), Zamin danesh Pars Engineering consultants, Tehran

Abrahamson N, Silva W (2008) Summary of the Abrahamson & Silva NGA Ground-Motion Relations Earthquake Spectra 24:67-97 doi:10.1193/1.2924360

Abrahamson NA, Bommer JJ (2005) Probability and Uncertainty in Seismic Hazard Analysis Earthquake Spectra 21:603-607 doi:10.1193/1.1899158

Abrahamson NA, Silva WJ, Kamai R (2014) Summary of the ASK14 Ground Motion Relation for Active Crustal Regions Earthquake Spectra 30:1025-1055 doi:10.1193/070913eqs198m

Ajalloeian R, Jami N (2010) Evaluation of engineering geology og Isfahan Quaternary deposits using Isfahan geotechnical data bank Journal of Science (Kharazmi University) 10:-

Akkar S, Cagnan Z (2010) A Local Ground-Motion Predictive Model for Turkey, and Its Comparison with Other Regional and Global Ground-Motion Models Bulletin of the Seismological Society of America 100:2978-2995 doi:10.1785/0120090367

Akkar S, Sandıkkaya MA, Bommer JJ (2014) Empirical ground-motion models for point- and extended-source crustal earthquake scenarios in Europe and the Middle East Bulletin of Earthquake Engineering 12:359-387 doi:10.1007/s10518-013-9461-4

Alavi M (1994) Tectonics of the zagros orogenic belt of iran: new data and interpretations Tectonophysics 229:211-238 doi:https://doi.org/10.1016/0040-1951(94)90030-2

Alipoor R, Zare M, Ghassemi M (2012) Inception of activity and slip rate on the Main Recent Fault of Zagros Mountains, Iran Geomorphology s 175–176:86–97 doi:10.1016/j.geomorph.2012.06.025

Allen T (2020) Seismic hazard estiation in stable continental regions: does PSHA meet the needs for modern engineering in Australia? Bulletin of the New Zealand Society for Earthquake Engineering 53:22-36 doi:10.5459/bnzsee.53.1.22-36

Ambraseys NN, Melville CP (1982) A history of Persian earthquakes Cambridge University Press, Cambridge:219 doi:doi:10.1002/eqe.4290110412

Anderson JG, Luco JE (1983) Consequences of slip rate constraints on earthquake occurrence relations Bulletin of the Seismological Society of America 73:471-496

Arian M (2015) Seismotectonic-Geologic Hazards Zoning of Iran Earth Sciences Research Journal 19:7-13

ASCE7 (2016) Minimum Design Loads for Buildings and Other Structures. Reston, VA

Atkinson G, Boore D (2007) Earthquake Ground-Motion Prediction Equations for Eastern North America Bulletin of the Seismological Society of America 96:2181-2205 doi:10.1785/0120050245

Baker J, Cornell C (2006) Spectral shape, epsilon and record selection Earthquake engineering and structural dynamics 35:1077–1095

Bazzurro P, Cornell C (1999) Disaggregation of Seismic Hazard Bulletin of Seismological Society of America 89:501-529

Bazzurro P, Cornell CA (2004) Nonlinear Soil-Site Effects in Probabilistic Seismic-Hazard Analysis Bulletin of the Seismological Society of America 94:2110-2123

Beauval C, Bard P-Y, Danciu L (2020) The influence of source- and ground-motion model choices on probabilistic seismic hazard levels at 6 sites in France Bulletin of Earthquake Engineering 18:4551-4580 doi:10.1007/s10518-020-00879-z

Berberian M (1979) Earthquake faulting and bedding thrust associated with the Tabas-e-Golshan (Iran) earthquake of September 16, 1978 Bulletin of the Seismological Society of America 69:1861-1887

Berberian M (2005) The 2003 Bam Urban Earthquake: A Predictable Seismotectonic Pattern along the Western Margin of the Rigid Lut Block, Southeast Iran Earthquake Spectra 21:35-99 doi:10.1193/1.2127909

Berberian M, King G (1981) Toward a pale geography and tectonic evolution of Iran Canadian Journal of Earth Sciences 18:210-265 doi:10.1139/e81-019

Beygi S, Nadimi A, Safaei H (2016) Tectonic history of seismogenic fault structures in Central Iran Journal of Geosciences 61:127-144

Bommer J, Crowley H (2017) The Purpose and Definition of the Minimum Magnitude Limit in PSHA Calculations Seismological Research Letters 88:1097-1106 doi:10.1785/0220170015

Boore DM, Stewart JP, Seyhan E, Atkinson GM (2014) NGA-West2 Equations for Predicting PGA, PGV, and 5% Damped PSA for Shallow Crustal Earthquakes Earthquake Spectra 30:1057-1085 doi:10.1193/070113eqs184m

Budnitz R, Apostolakis G, Boore D, Cluff L, Coppersmith K, Cornell C, Morris P (1997) Recommendations for Probabilistic Seismic Hazard Analysis: Guidance on Uncertainty and Use of Experts: Main Report vol 1.

Calais E, Camelbeeck T, Stein S, Liu M, Craig TJ (2016) A new paradigm for large earthquakes in stable continental plate interiors Geophysical Research Letters 43:10,621-610,637 doi:https://doi.org/10.1002/2016GL070815

Campbell KW, Bozorgnia Y (2014) NGA-West2 Ground Motion Model for the Average Horizontal Components of PGA, PGV, and 5% Damped Linear Acceleration Response Spectra Earthquake Spectra 30:1087-1115 doi:10.1193/062913eqs175m

Cauzzi C, Faccioli E, Vanini M, Bianchini A (2015) Updated predictive equations for broadband (0.01–10 s) horizontal response spectra and peak ground motions, based on a global dataset of digital acceleration records Bulletin of Earthquake Engineering 13:1587-1612 doi:10.1007/s10518-014-9685-y

Chiou B-J, Youngs RR (2008) An NGA Model for the Average Horizontal Component of Peak Ground Motion and Response Spectra Earthquake Spectra 24:173-215 doi:10.1193/1.2894832

Chiou BS-J, Youngs RR (2014) Update of the Chiou and Youngs NGA Model for the Average Horizontal Component of Peak Ground Motion and Response Spectra Earthquake Spectra 30:1117-1153 doi:10.1193/072813eqs219m

Cornell CA (1968) Engineering seismic risk analysis Bulletin of Seismological Society of America 58:1583-1606

Craig T, Calais E, Fleitout L, Bollinger L, Scotti O (2016) Evidence for the release of long-term tectonic strain stored in continental interiors through intraplate earthquakes Geophysical Research Letters 43 doi:10.1002/2016GL069359

Crowley H, Bommer JJ, Pinho R, Bird J (2005) The impact of epistemic uncertainty on an earthquake loss model Earthquake Engineering & Structural Dynamics 34:1653-1685 doi:doi:10.1002/eqe.498

Danciu L, Kale Ö, Akkar S (2016a) The 2014 Earthquake Model of the Middle East: ground motion model and uncertainties Bulletin of Earthquake Engineering:1-37 doi:10.1007/s10518-016-9989-1

Danciu L, Sesetyan K, Demircioglu M, Erdik M, Giardini D (2016b) OpenQuake input files of the Seismogenic Source Model of the 2014 Earthquake Model of the Middle East (EMME-Project) doi:10.12686/a3

Danciu L et al. (2017) The 2014 Earthquake Model of the Middle East: seismogenic sources Bulletin of Earthquake Engineering:1-32 doi:10.1007/s10518-017-0096-8

Darzi A, Zolfaghari MR, Cauzzi C, Fäh D (2019) An Empirical Ground-Motion Model for Horizontal PGV, PGA, and 5% Damped Elastic Response Spectra (0.01–10 s) in Iran Bulletin of the Seismological Society of America 109:1041-1057 doi:10.1785/0120180196

Douglas J, Edwards B (2016) Recent and future developments in earthquake ground motion estimation Earth-Science Reviews 160:203-219 doi:https://doi.org/10.1016/j.earscirev.2016.07.005

Ebrahimian H et al. (2019) Site-specific probabilistic seismic hazard analysis for the western area of Naples, Italy Bulletin of Earthquake Engineering 17:4743-4796 doi:10.1007/s10518-019-00678-1

Eftekharnejad J (1981) Tectonic division of Iran with respect to sedimentary basins Journal of Iranian Petroleum Society 82:19-28

Fallah Tafti M, Amini Hosseini K, Firouzi E, Mansouri B, Ansari A (2017) Ranking of GMPEs for Seismic Hazard Analysis in Iran Using LH, LLH and EDR Approaches Journal of seismology and earthquake engineering 19

Farajpour Z, Kowsari M, Pezeshk S, Halldorsson B (2020) Ranking of Ground-Motion Models (GMMs) for Use in Probabilistic Seismic Hazard Analysis for Iran Based on an Independent Data Set Bulletin of the Seismological Society of America doi:10.1785/0120200052

Farajpour Z, Pezeshk S, Zare M (2019) A New Empirical Ground-Motion Model for Iran Bulletin of the Seismological Society of America xx doi:10.1785/0120180139

Farashi S, Ajalloeian R (2012) Engineering geological mapping at east of Isfahan city using GIS 6:165-172

Field E, Jordan T, Cornell CA (2003) OpenSHA: A Developing Community-modeling Environment for Seismic Hazard Analysis Seismological Research Letters 74:406-419

Fossen H (2010) Structural Geology. First Edition edn. Cambridge University Press,

Frankel A (1995) Mapping Seismic Hazard in the Central and Eastern United States Seismological Research Letters 66:8-21 doi:10.1785/gssrl.66.4.8

Gardner J, Knopoff L (1974) Is the sequence of earthquakes in southern California, with aftershocks removed, Poissonian Bulletin of the Seismological Society of America 64:1363–1367

Ghasemi A, Talbot CJ (2006) A new tectonic scenario for the Sanandaj–Sirjan Zone (Iran) Journal of Asian Earth Sciences 26:683-693 doi:https://doi.org/10.1016/j.jseaes.2005.01.003

Ghasemi H, Zare M, Fukushima Y, Koketsu K (2009) An empirical spectral ground-motion model for Iran Journal of Seismology 13:499-515 doi:10.1007/s10950-008-9143-x

Giardini D (1999) The Global Seismic Hazard Assessment Program (GSHAP) - 1992/1999 1999 42 doi:10.4401/ag-3780

Hanks TC, Kanamori H (1979) A moment magnitude scale Journal of Geophysical Research: Solid Earth 84:2348-2350 doi:https://doi.org/10.1029/JB084iB05p02348

Hassanpour J, Jahani S, Ghassemi M, Alavi A, Zeinali F (2018) Evolution of the Karebas Fault System and adjacent folds, central Zagros fold-and-thrust belt, Iran: Role of pre-existing halokinesis (salt structures and minibasins) and detachment levels Journal of Asian Earth Sciences 164:125–142 doi:10.1016/j.jseaes.2018.06.024

Hofmann RB (1996) Individual faults can't produce a Gutenberg-Richter earthquake recurrence Engineering Geology 43:5-9 doi:https://doi.org/10.1016/0013-7952(95)00085-2

ICSRDB (2014) Iranian Code of Practice for Earthquake Resistant Design of Buildings (Standard 2800), 4th Edition. PN S 253, Building and Housing Research Center of Iran,

Jackson J, Haines J, Holt W (1995) The accommodation of Arabia-Eurasia Plate convergence in Iran Journal of Geophysical Research: Solid Earth 100:15205-15219 doi:https://doi.org/10.1029/95JB01294

Jamali F, Hessami K (2011) Active tectonics and strain partitioning along dextral fault system in Central Iran: Analysis of geomorphological observations and geophysical data in the Kashan region Journal of Asian Earth Sciences - J ASIAN EARTH SCI 40:1015-1025 doi:10.1016/j.jseaes.2010.05.013

Johnston A, Kanter L, Coppersmith K, Cornell C (1994) The Earthquakes of Stable Continental Regions. EPRI TR-102261, five volumes. JF Schneider (ed.), final proprietary report for the Electric Power Research Institute, Palo Alto, California.

Kalaneh S, Agh-Atabai M (2016) Spatial variation of earthquake hazard parameters in the Zagros fold and thrust belt, SW Iran Natural Hazards 82:933-946 doi:10.1007/s11069-016-2227-y

Kale Ö, Akkar S (2013) A New Procedure for Selecting and Ranking Ground-Motion Prediction Equations (GMPEs): The Euclidean Distance-Based Ranking (EDR) Method The Bulletin of the Seismological Society of America 103:1069-1084 doi:10.1785/0120120134

Kale Ö, Akkar S, Ansari A, Hamzehloo H (2015) A Ground-Motion Predictive Model for Iran and Turkey for Horizontal PGA, PGV, and 5% Damped Response Spectrum: Investigation of Possible Regional Effects Bulletin of the Seismological Society of America 105:963-980 doi:10.1785/0120140134

Karasozen E, Nissen E, Bergman E, Ghods A (2018) A bias-free seismicity catalog for the entire Zagros (Iran) orogeny. December 01, 2018

Khodaverdian A, Zafarani H, Rahimain M (2015) Long term Fault slip rates, distributed deformation rates and forecast of seismicity in the Iranian Plateau Tectonics 34 doi:10.1002/2014TC003796

Khorrami F et al. (2019) An up-to-date crustal deformation map of Iran using integrated campaign-mode and permanent GPS velocities Geophysical Journal International 217 doi:10.1093/gji/ggz045

Kijko A (2004) Estimation of the Maximum Earthquake Magnitude,mmax Pure and Applied Geophysics 161:1655-1681 doi:10.1007/s00024-004-2531-4

Kohrangi M, Danciu L, Bazzurro P (2018) Comparison between outcomes of the 2014 Earthquake Hazard Model of the Middle East (EMME14) and national seismic design codes: The case of Iran Soil Dynamics and Earthquake Engineering 114:348-361 doi:https://doi.org/10.1016/j.soildyn.2018.07.022

Leonard M (2010) Earthquake Fault Scaling: Self-Consistent Relating of Rupture Length, Width, Average Displacement, and Moment Release Bulletin of the Seismological Society of America 100:1971-1988 doi:10.1785/0120090189

Leonard M (2014) Self-Consistent Earthquake Fault-Scaling Relations: Update and Extension to Stable Continental Strike-Slip Faults Bulletin of the Seismological Society of America 104:2953-2965 doi:10.1785/0120140087

Lin P-S, Lee C-T (2008) Ground-Motion Attenuation Relationships for Subduction-Zone Earthquakes in Northeastern Taiwan Bulletin of the Seismological Society of America 98:220-240 doi:10.1785/0120060002

McGuire RK (2004) Seismic hazard and risk analysis. Earthquake Engineering Research Institute,

McQuarrie N (2004) Crustal scale geometry of the Zagros fold–thrust belt, Iran Journal of Structural Geology 26:519-535 doi:https://doi.org/10.1016/j.jsg.2003.08.009

Mignan A, Danciu L, Giardini D (2015) Reassessment of the Maximum Fault Rupture Length of Strike-Slip Earthquakes and Inference on Mmax in the Anatolian Peninsula, Turkey Seismological Research Letters 86:890-900 doi:10.1785/0220140252

Mohajjel M, Fergusson CL (2000) Dextral transpression in Late Cretaceous continental collision, Sanandaj–Sirjan Zone, western Iran Journal of Structural Geology 22:1125-1139 doi:https://doi.org/10.1016/S0191-8141(00)00023-7

Mohammadi M, Fatemi Aghda SM, talkhablou M, Cheshomi A (2020) The subsurface development and geological and geotechnical characteristics of coarse-grained sediments of Zayandeh rood river in Isfahan city Journal of Geoscience 30:231-242 doi:10.22071/gsj.2020.208126.1720

Moinfar AA, Naderzadeh A, Nabavi MH (2012) New Iranian Seismic Hazard Zoning Map for New Edition of Seismic Code and Its Comparison with Neighbor Countries. Paper presented at the 15th WCEE, Lisbon, Portugal,

Mousavi M, Ansari A, Zafarani H, Azarbakht A (2012) Selection of Ground Motion Prediction Models for Seismic Hazard Analysis in the Zagros Region, Iran Journal of Earthquake Engineering - J EARTHQU ENG 16 doi:10.1080/13632469.2012.685568

Nogole-Sadat M, Almasian M (1993) Tectonic Map of Iran, Scale 1:1,000,000 Geological Survey of Iran

Nowroozi AA (1985) Empirical relations between magnitudes and fault parameters for earthquakes in Iran Bulletin of the Seismological Society of America 75:1327-1338

Oveisi B, Sabour N, Sadeghi M, Heibati Z (2019) Seismotectonic Map of Iran (GIS-Ready). doi:10.13140/RG.2.2.34188.26248

Pagani M et al. (2014) OpenQuake Engine: an Open Hazard (and Risk) Software for the Global Earthquake Model Seismol Res Lett 85:692–702

Papadopoulos G, Baskoutas I, Fokaefs A (2014) Historical seismicity of the Kyparissiakos Gulf, western Peloponnese, Greece Bollettino di Geofisica Teorica ed Applicata 55:389-404 doi:10.4430/bgta0096

Pezeshk S, Zandieh A, Tavakoli B (2011) Hybrid Empirical Ground-Motion Prediction Equations for Eastern North America Using NGA Models and Updated Seismological Parameters Bulletin of The Seismological Society of America - BULL SEISMOL SOC AMER 101:1859-1870 doi:10.1785/0120100144

Poggi V, Garcia-Peláez J, Styron R, Pagani M, Gee R (2020) A probabilistic seismic hazard model for North Africa Bulletin of Earthquake Engineering 18:2917-2951 doi:10.1007/s10518-020-00820-4

Reiter L (1992) Earthquake Hazard Analysis: Issues and insights Surveys in Geophysics 13:297-298 doi:10.1007/BF02125772

Rodriguez-Marek A, Rathje EM, Bommer JJ, Scherbaum F, Stafford PJ (2014) Application of Single-Station Sigma and Site-Response Characterization in a Probabilistic Seismic-Hazard Analysis for a New Nuclear Site Bulletin of the Seismological Society of America 104:1601-1619 doi:10.1785/0120130196

Safaei H (2009) The continuation of the Kazerun fault system across the Sanandaj–Sirjan zone (Iran) Journal of Asian Earth Sciences 35:391-400 doi:https://doi.org/10.1016/j.jseaes.2009.01.007

Safaei H, Tabatabaeimanesh SM, Hashemi SN, Mirlohi AS, Vafa H (2012) Structural and petrological evidence for the continuation of the Isfahan fault system across the Urumieh-Dokhtar zone of central Iran Geotectonics 46:455-471 doi:10.1134/s0016852112060064

Scasserra G, Stewart JP, Bazzurro P, Lanzo G, Mollaioli F (2009) A Comparison of NGA Ground-Motion Prediction Equations to Italian Data Bulletin of the Seismological Society of America 99:2961-2978 doi:10.1785/0120080133

Scordilis EM (2006) Empirical Global Relations Converting MS and mb to Moment Magnitude Journal of Seismology 10:225-236 doi:10.1007/s10950-006-9012-4

Sedaghati F, Pezeshk S (2017) Partially Nonergodic Empirical Ground-Motion Models for Predicting Horizontal and Vertical PGV, PGA, and 5% Damped Linear Acceleration Response Spectra Using Data from the Iranian Plateau Bulletin of the Seismological Society of America 107:934-948 doi:10.1785/0120160205

Şengör AMC (1990) A new model for the late Palaeozoic—Mesozoic tectonic evolution of Iran and implications for Oman Geological Society, London, Special Publications 49:797-831 doi:10.1144/gsl.sp.1992.049.01.49

Sepehr M, Cosgrove J (2004) Structural framework of the Zagros Fold–Thrust Belt, Iran Marine and Petroleum Geology 21:829-843 doi:10.1016/j.marpetgeo.2003.07.006

Şeşetyan K et al. (2018) The 2014 seismic hazard model of the Middle East: overview and results Bulletin of Earthquake Engineering doi:10.1007/s10518-018-0346-4

Shahjouei A, Pezeshk S (2016) Alternative Hybrid Empirical Ground-Motion Model for Central and Eastern North America Using Hybrid Simulations and NGA-West2 Models Bulletin of the Seismological Society of America 106 doi:10.1785/0120140367

Sonley E, Atkinson G (2005) Empirical Relationship between Moment Magnitude and Nuttli Magnitude for Small-magnitude Earthquakes in Southeastern Canada Seismological Research Letters - SEISMOL RES LETT 76:752-755 doi:10.1785/gssrl.76.6.752

Stepp J Analysis of completeness of the earthquake sample in the Puget Sound area and its effect on statistical estimates of earthquake hazard. In: Proceedings of the International Conference on Microzonation, 1972. pp 897-910

Tabaei M, Mehdizadeh R, Esmaeili M (2016) Stratigraphical evidences of the Qom – Zefreh Fault system activity, Central Iran 4:18-26

Tajmir Riahi Z, Ajalloeian R, Rahgozar MA, Safaei H (2014) Earthquake Hazard Zonation of the Isfahan City, Iran Journal of Geotechnical Engineering 19:7141-7163

Talebian M, Jackson J (2004) A reappraisal of earthquake focal mechanisms and active shortening in the Zagros Mountains of Iran Geophysical Journal International 156:506-526 doi:10.1111/j.1365-246X.2004.02092.x

Vernant P et al. (2004) Deciphering oblique shortening of central Alborz in Iran using geodetic data Earth and Planetary Science Letters 223:177-185 doi:https://doi.org/10.1016/j.epsl.2004.04.017

Vilanova S et al. (2014) Incorporating Descriptive Metadata into Seismic Source Zone Models for Seismic-Hazard Assessment: A Case Study of the Azores-West Iberian Region Bulletin of the Seismological Society of America 104:1212-1229 doi:10.1785/0120130210

Wald DJ, Allen TI (2007) Topographic Slope as a Proxy for Seismic Site Conditions and Amplification Bulletin of the Seismological Society of America 97:1379-1395 doi:10.1785/0120060267

Walpersdorf A et al. (2014) Present-day kinematics and fault slip rates in eastern Iran, derived from 11 years of GPS data Journal of Geophysical Research: Solid Earth 119:1359-1383 doi:https://doi.org/10.1002/2013JB010620

Weichert DH (1980) Estimation of the earthquake recurrence parameters for unequal observation periods for different magnitudes Bulletin of the Seismological Society of America 70:1337-1346

Wells D, Coppersmith K (1994) New Empirical Relationships among Magnitude, Rupture Length, Rupture Width, Rupture Area, and Surface Displacement Bulletin of the Seismological Society of America 84:974-1002

Wesnousky SG, Scholz CH, Shimazaki K, Matsuda T (1983) Earthquake frequency distribution and the mechanics of faulting Journal of Geophysical Research: Solid Earth 88:9331-9340 doi:https://doi.org/10.1029/JB088iB11p09331

Youngs RR, Chiou S-J, Silva WJ, Humphrey JR (1997) Strong Ground Motion Attenuation Relationships for Subduction Zone Earthquakes Seismological Research Letters 68:58-73 doi:10.1785/gssrl.68.1.58

Zafarani H, Luzi L, Lanzano G, Soghrat MR (2018) Empirical equations for the prediction of PGA and pseudo spectral accelerations using Iranian strong-motion data Journal of Seismology 22:263-285 doi:10.1007/s10950-017-9704-y

Zafarani H, Mousavi M (2014) Applicability of different ground-motion prediction models for northern Iran Natural Hazards 73:1199-1228 doi:10.1007/s11069-014-1151-2

Zare M et al. (2014) Recent developments of the Middle East catalog Journal of Seismology 18 doi:10.1007/s10950-014-9444-1

Zhao JX et al. (2006) Attenuation Relations of Strong Ground Motion in Japan Using Site Classification Based on Predominant Period Bulletin of the Seismological Society of America 96:898-913 doi:10.1785/0120050122

Zöller G, Holschneider M, Hainzl S (2013) The Maximum Earthquake Magnitude in a Time Horizon: Theory and Case Studies Bulletin of the Seismological Society of America 103:860-875 doi:10.1785/0120120013

Figures

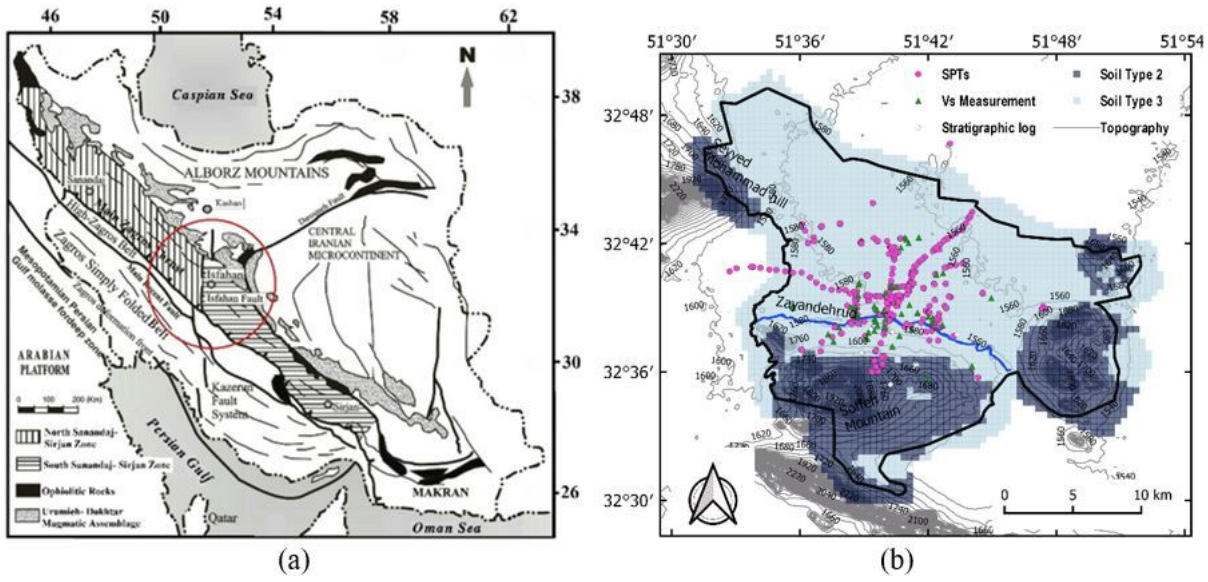

Figure 1

(a) Summary of tectonic map of Iran adapted from Safaei et al. (2012). According to this map, the study area is mostly located in the North Sanandaj-Sirjan zone, in the South Sanadaj-Sirjan and partially in the high Zagros belt, Zagros simply folded belt, Urumieh-Dokhtar magmatic assemblage and Central Iran (Note: the red circle indicates 200 km distance from Isfahan); (b) Geotechnical setting of Isfahan showing the boundaries of the soil types, topography, and the location and type of the available geotechnical test data.

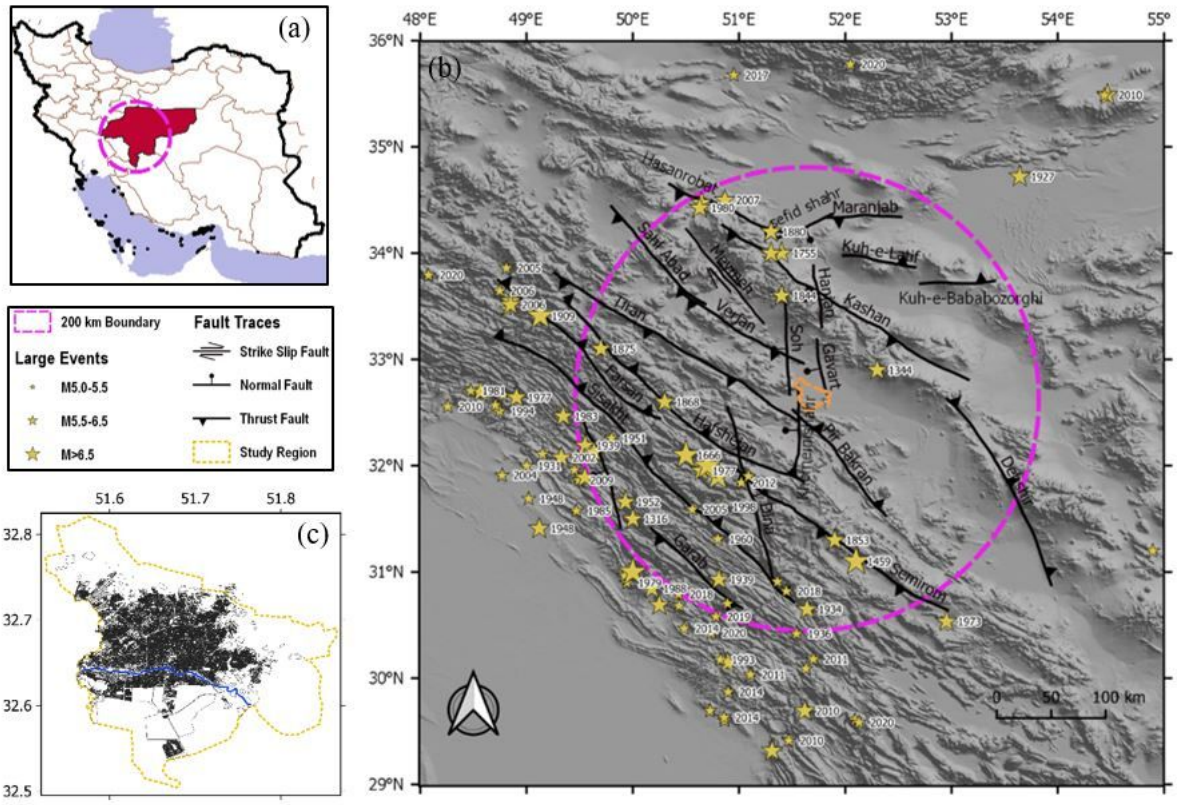

Figure 2

(a) Map of Iran and the boundaries of the Isfahan province (red area); (b) Tectonic and seismological setting of the region, the location of the case-study region, main faults, and historical earthquakes with Mw≥5.0; (c) the extents of the urban area of Isfahan and the extension of the living areas of the city.

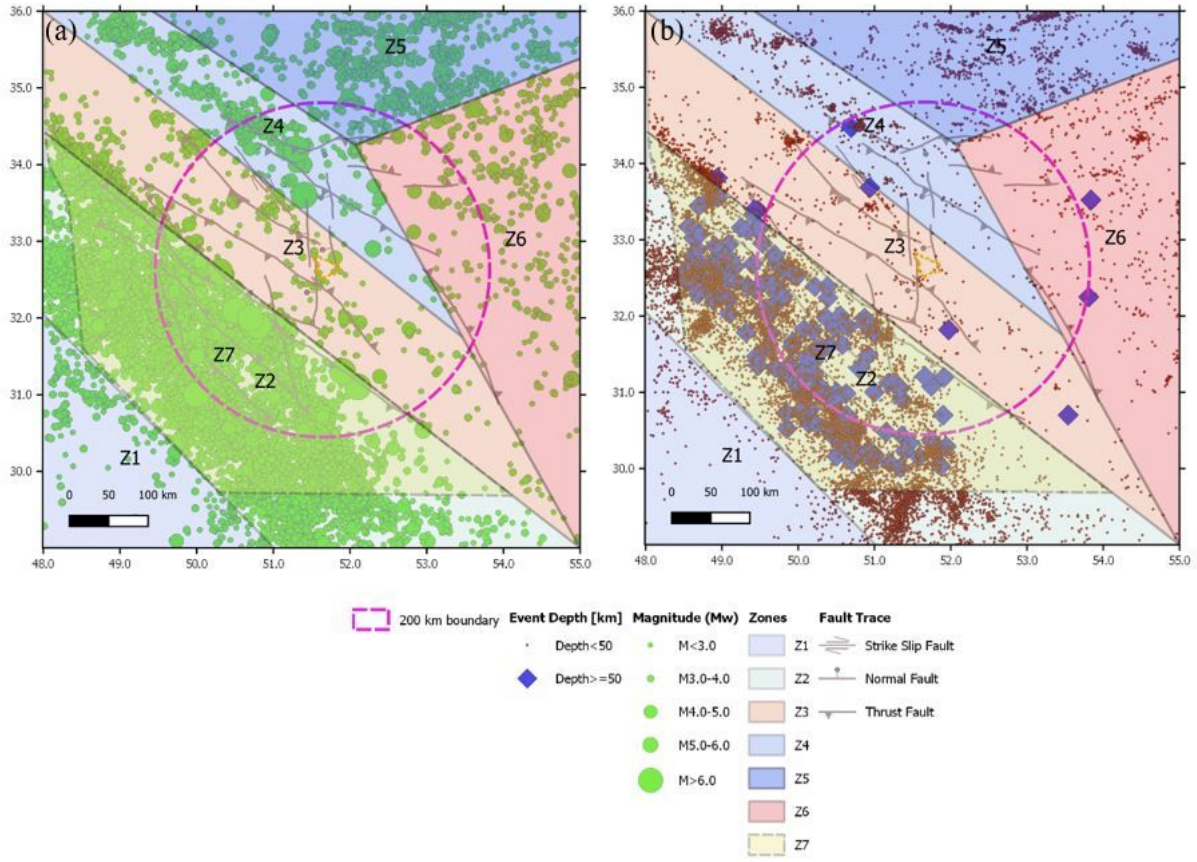

Figure 3

Delineation of the boundaries of the proposed source zonation of Isfahan with the catalogue showing the spatial distribution of the events in terms of: (a) event moment magnitudes; and (b) hypo-central depth. Note: The fault traces and fault mechanisms are also shown on the maps.

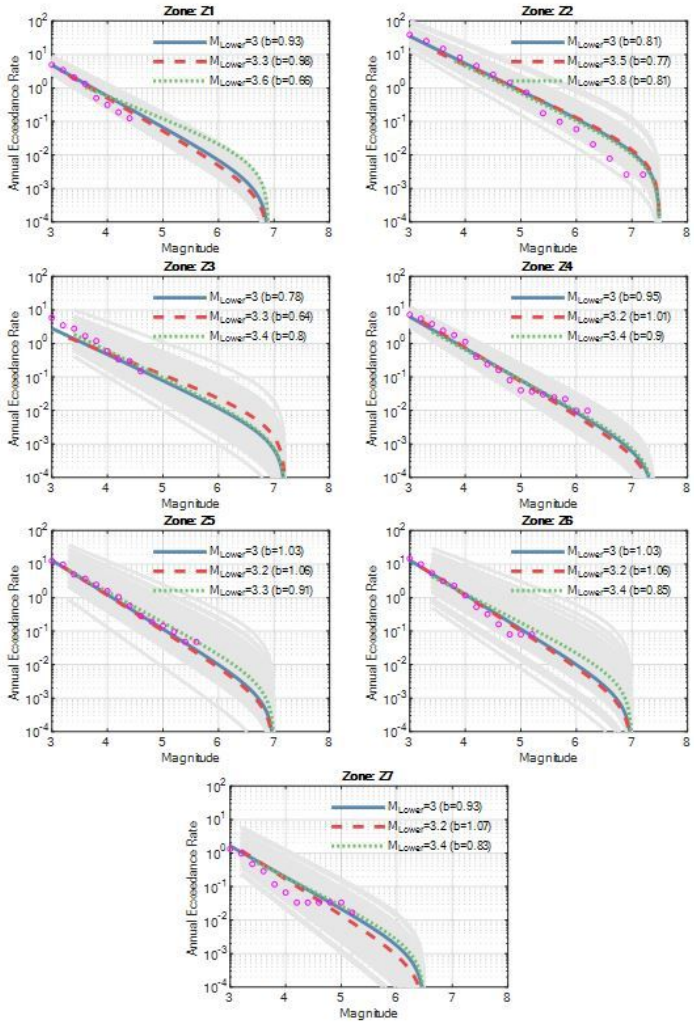

Figure 4

Magnitude occurrence relations of the Isfahan seismicity model for the seven delineated zones. Note that the grey lines are 100 realizations of the curve fit using a distribution around bGR and the circle markers show the observed number of events.

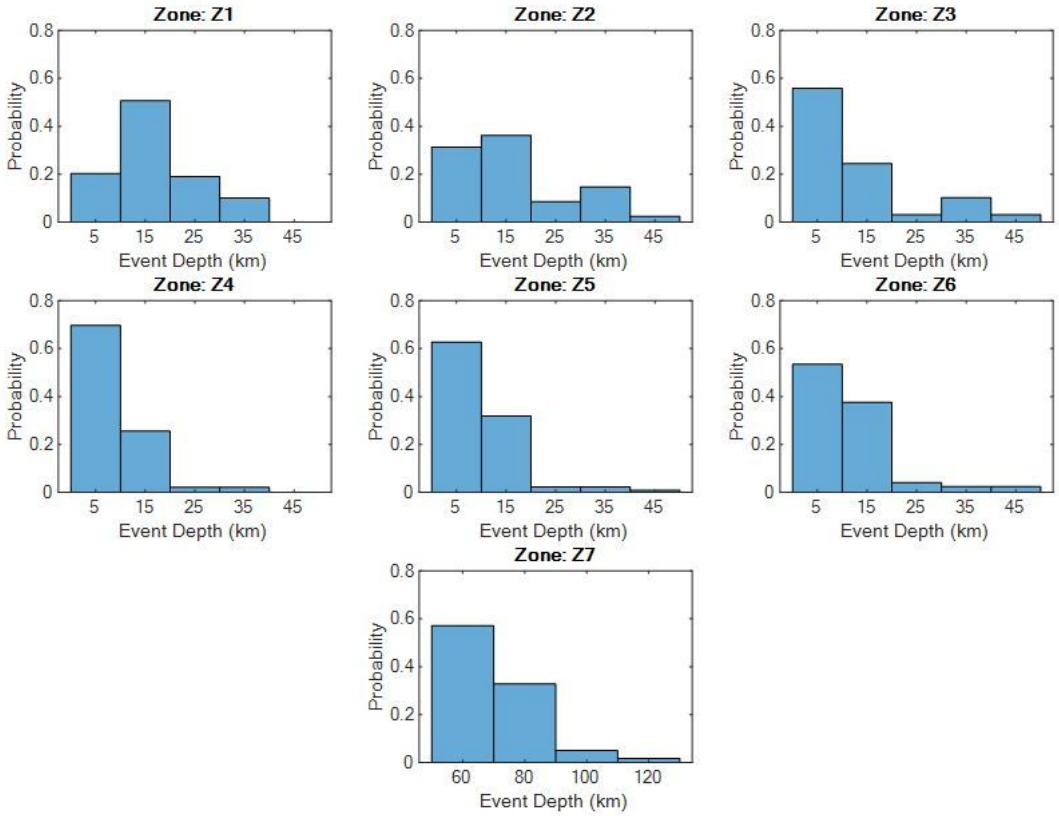

Figure 5

Earthquake hypo-central depth distribution of the seven seismic zones of Isfahan source model.

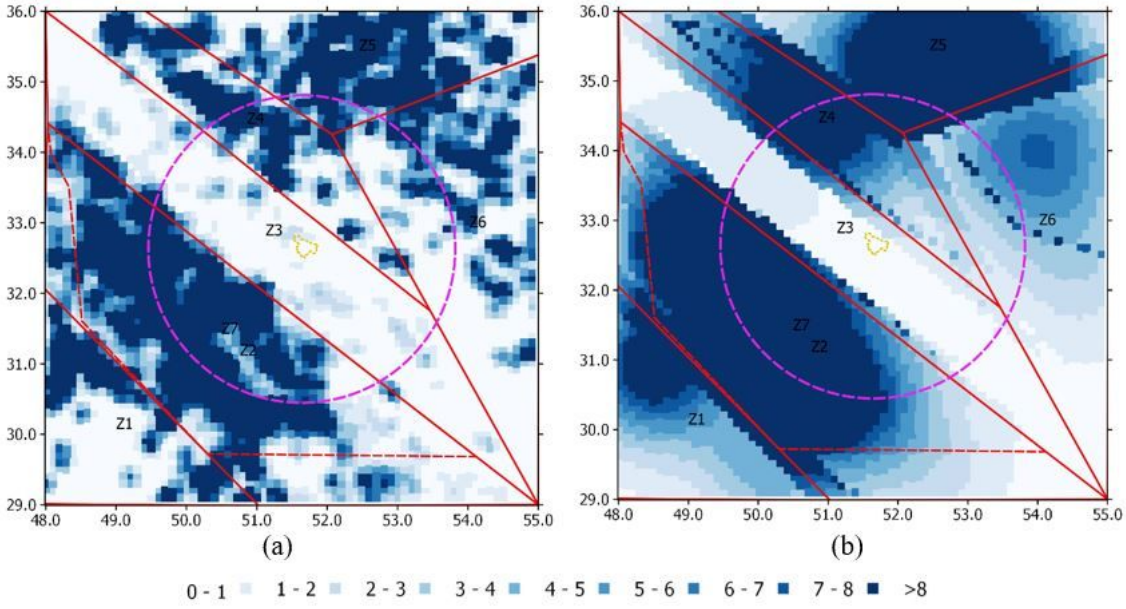

Figure 6

Spatial redistribution of the cumulative annual rates (Mw>0) within unit area 0.1°×0.1° (about 11 km2) based on: (a) Cd=10 km; (b) Cd=70 km. Note: These maps also show the extents of the zones and the 200 km boundary around Isfahan.

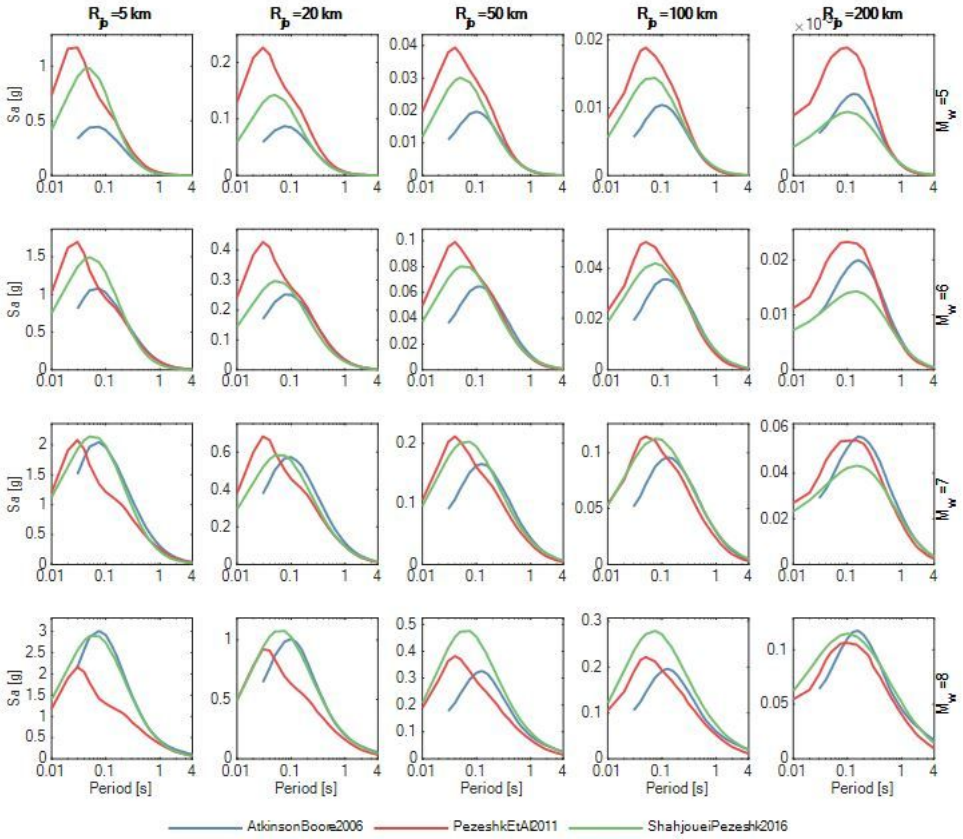

Figure 7

Trellis plots for the three GMPEs of AB06, PZT11 and SP16 for different scenarios in the stable continental region.

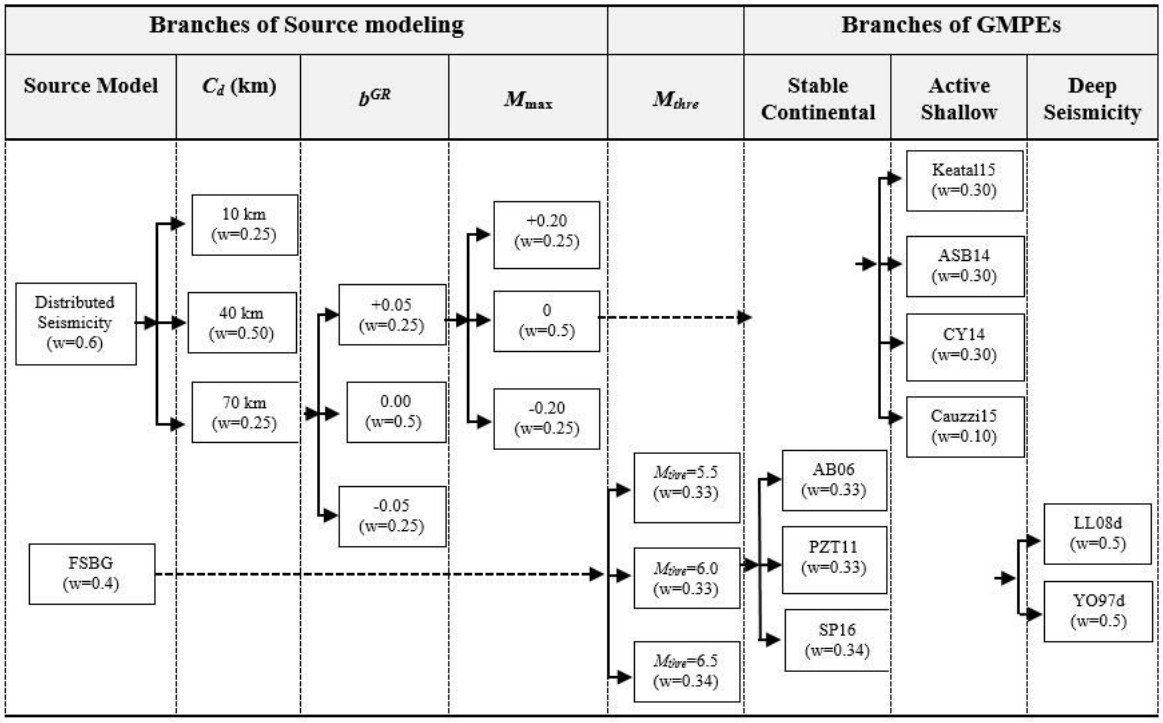

Figure 8

Logic tree structure used in the PSHA of this study

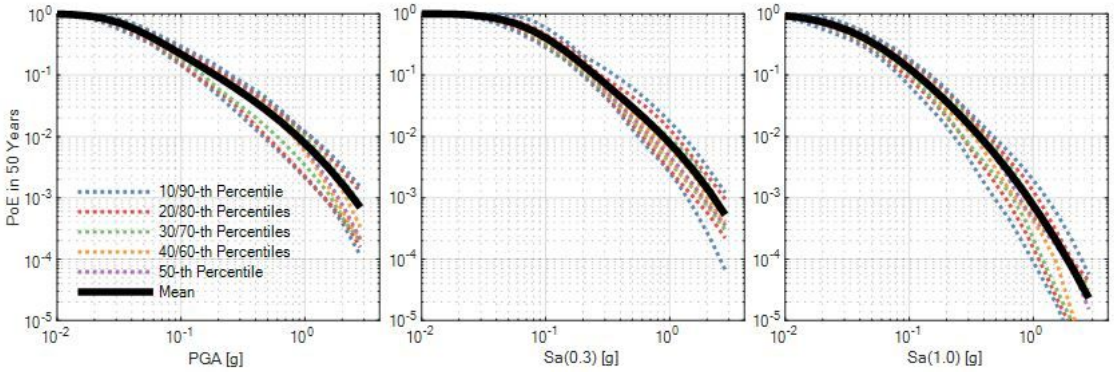

Figure 9

Seismic hazard curves (mean and percentiles) for PGA, and spectral accelerations at 0.3s and 1.0s for a selected site in Isfahan urban area with soil conditions characterized by a Vs30 map.

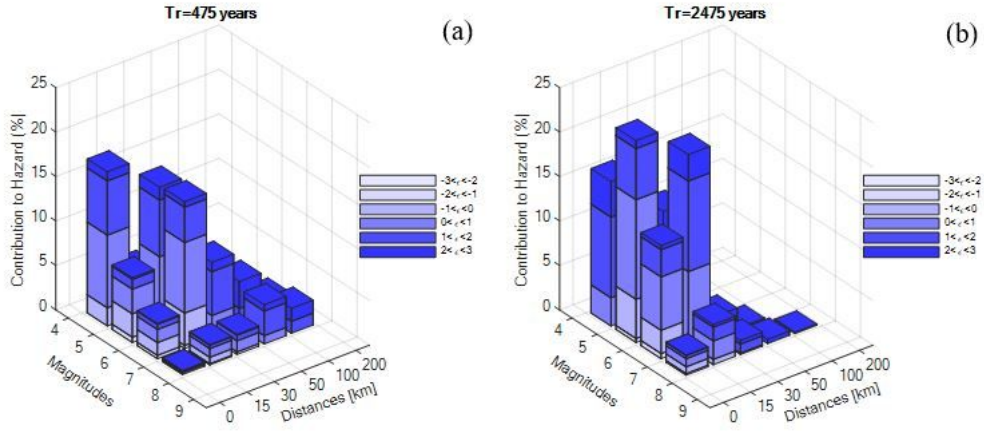

Figure 10

Disaggregation results for: (a) Tr=475; and, (b) Tr=2,475 years for PGA. Note: epsilon (ε) represents the number of standard deviations from the (log) mean value of the GMPE. For more details about its definition, refer to Baker and Cornell (2006)

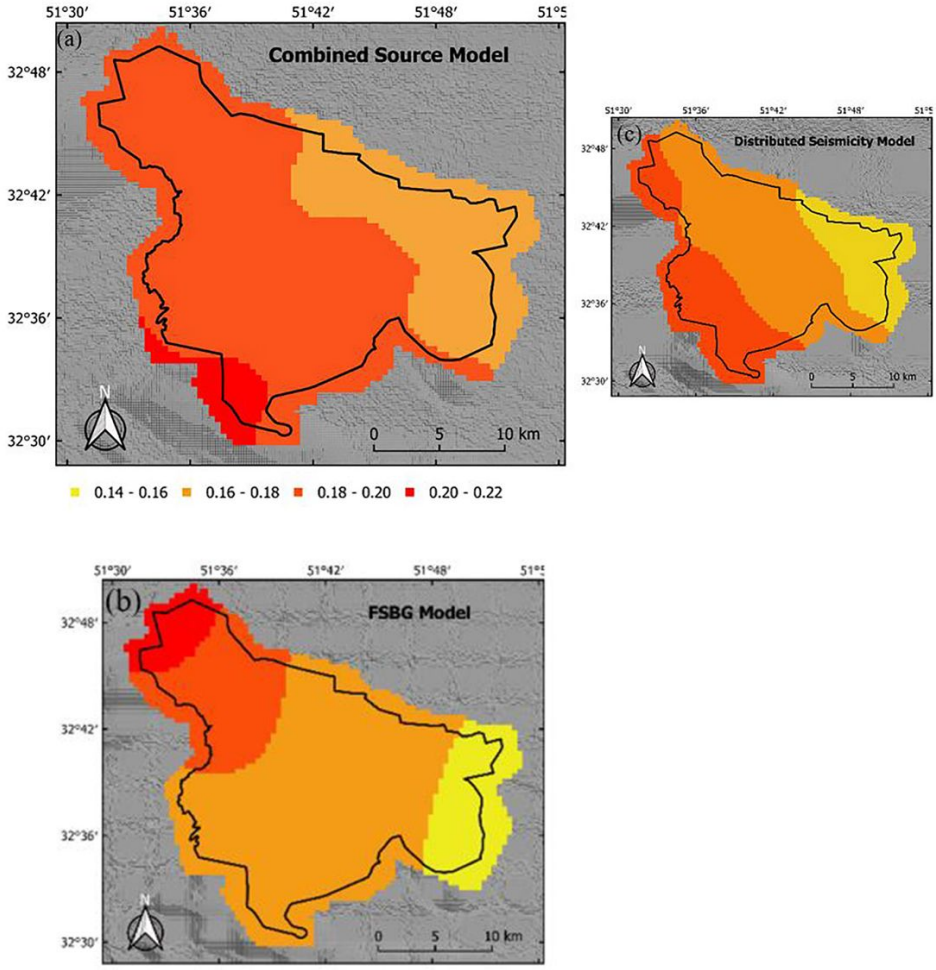

Figure 11

Mean hazard maps of PGA [g] on reference rock (Vs30=800 m/s) corresponding to the hazard level characterized by 10% probability of exceedance in 50 years (Tr=475) based on: (a) combined source model; (b) faults and background seismicity model; and, (c) distributed seismicity model.

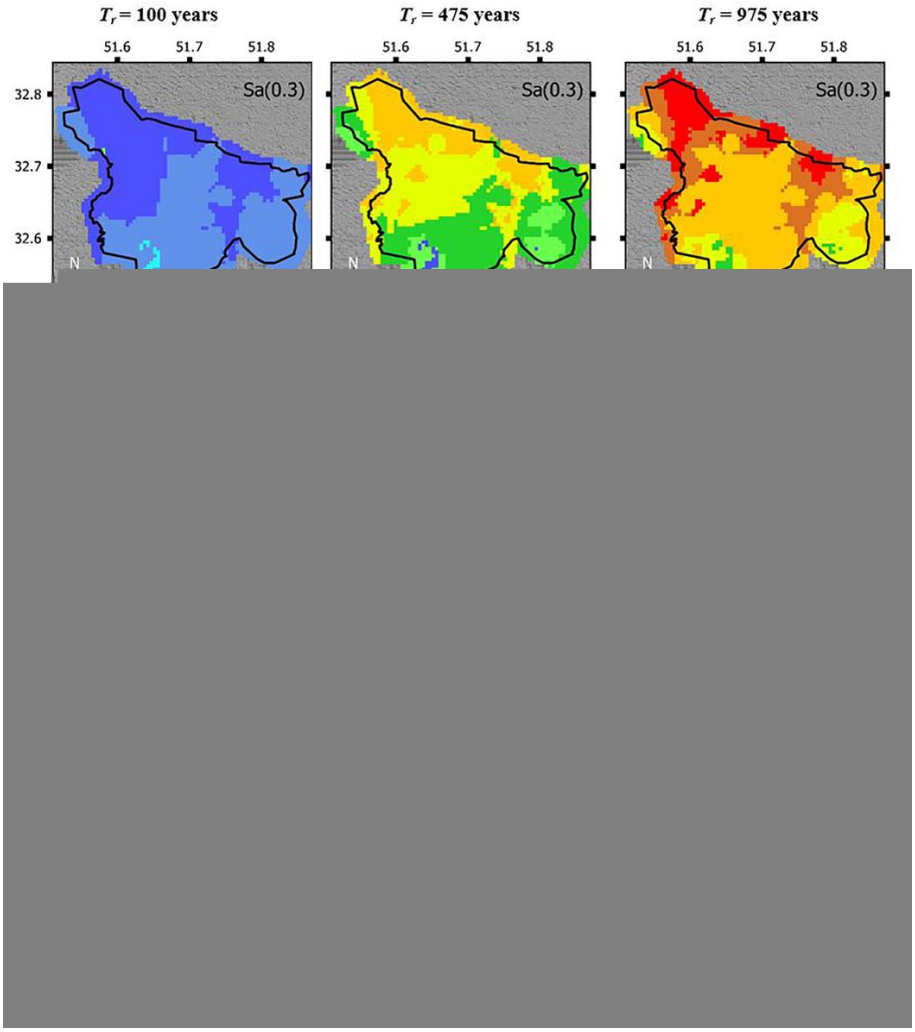

Figure 12

Mean hazard maps of Sa(0.3s), Sa(0.75s) and Sa(1.5s) [g] on soil corresponding to different hazard levels: Left column: 39% probability of exceedance in 50 years (Tr=100); Middle column: 10% probability of exceedance in 50 years (Tr=475); Right column: 5% probability of exceedance in 50 years (Tr=975).

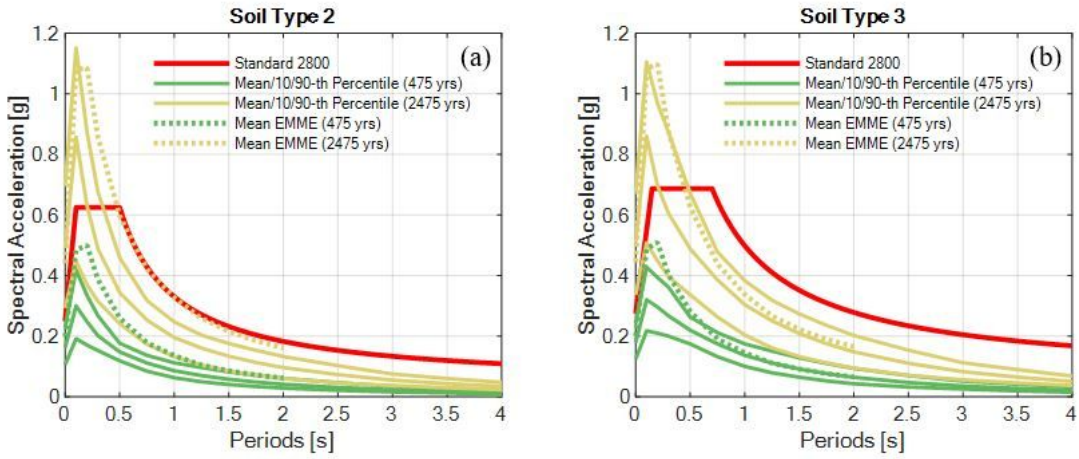

Figure 13

Comparison between mean uniform hazard spectrum for 10% in 50 years (Tr=475) and 2% in 50 years (Tr=2475) based on EMME14 and this study versus the design spectrum based on Standard 2800. Note: The UHS for a given soil type show the mean UHS of all sites with that soil category. The EMME14 UHS are truncated because the GMPEs utilized in the logic tree does not consider spectral accelerations beyond T=2.0s.

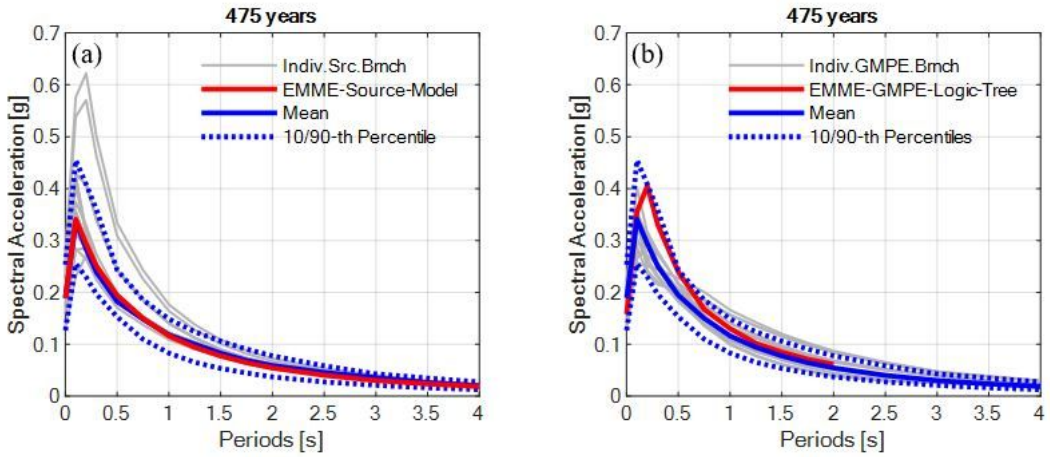

Figure 14

Contribution of individual branches of the logic tree on the UHS showing: (a) Individual source models (grey lines), full logic tree of this study (blue lines) and a combination of EMME source model with the GMPE logic tree of this study (red line); (b) individual GMPE branches (grey lines), full logic tree of this study (blue lines) and a combination of the source model of this study with the GMPE logic tree proposed by EMME (red line). Note: the EMME UHS are truncated to T=2.0s because of limitations in the GMPEs adopted in that study.

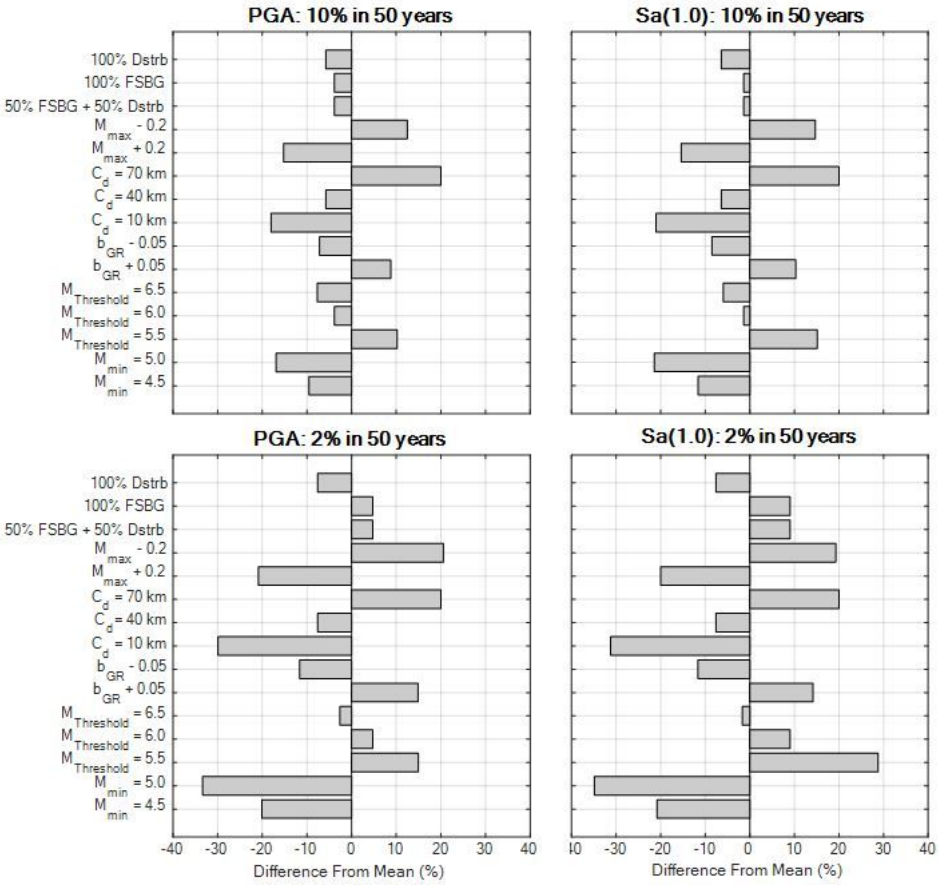

Figure 15

Tornado plot of percentage difference between the mean hazard estimates for PGA, left, and Sa(1.0), right, corresponding to Tr=475 years, top, and Tr=2,475 years, bottom.

Supplementary Files

This is a list of supplementary files associated with this preprint. Click to download.

- Supplementarymaterialr1d8.docx